MYC Targeted Rad50 Drives Progression of High-Grade Serous Ovarian Cancer via NF-κB Activation

Yinuo Li
Shandong University Qilu Hospital
Shourong Wang
Shandong University Qilu Hospital
Peng Li
Shandong University Qilu Hospital
Yingwei Li
Shandong University Cheeloo College of Medicine
Yao Liu
Shandong University Qilu Hospital
Haiya Fang
Jinhua Hospital of Zhejiang University: Jinhua Municipal Central Hospital
Xiyu Zhang
Shandong University Cheeloo College of Medicine
Zhaojian Liu (liujian9782@sdu.edu.cn)
Shandong University Cheeloo College of Medicine
Beihua Kong
Shandong University Qilu Hospital

Research

Keywords: MYC, Rad50, NF-κB, CARD9, ovarian cancer

Posted Date: November 24th, 2020

DOI: https://doi.org/10.21203/rs.3.rs-111959/v1

Abstract

Background

Rad50 is a component of MRN complex, which consists of Mre11-Rad50-Nbs1. The MRN complex participates in DNA double-strand break repair and DNA-damage checkpoint activation. We sought to investigate the clinical and functional significance of Rad50 in high-grade serous ovarian cancer.

Methods

Chromatin immunoprecipitation and luciferase assays were performed to evaluate the regulatory roles of MYC on Rad50 expression. Association between Rad50 expression and clinical outcome in HGSOCs was evaluated by Kaplan-Meier analysis. Invasion, clonogenic assay and xenograft mice model were conducted to determine to functional role of Rad50 in ovarian cancer. Protein immunoprecipitation and immunofluorescence were used to explore the underlying mechanisms.

Results

MYC proto-oncogene transcriptionally activated Rad50 expression in high-grade serous ovarian cancer. Next, we provided evidences that Rad50 was frequently upregulated in HGSOCs and enhanced Rad50 expression inversely correlated with patient's survival. In addition, ectopic expression of Rad50 promoted proliferation/invasion and induced EMT of ovarian cancer cells, whereas knockdown of Rad50 led to decreased aggressive behaviors. Mechanistic investigations revealed that Rad50 induced aggressiveness in HGSOC via activation NF-κB signaling pathway. Moreover, we identified CARD9 as an interacting protein of Rad50 in ovarian cancer cells and activation of NF-κB pathway by Rad50 is CARD9 dependent.

Conclusions

Our findings provide evidence that MYC targeted Rad50 exhibits oncogenic property via NF-κB activation in high-grade serous ovarian cancer.

Background

Ovarian cancer is the most lethal gynecologic malignancy and the overall 5-year survival rate is around 30% [1]. High-grade serous ovarian carcinoma (HGSOC) is the most common subtype and accounts for up to 70% of all ovarian cancer cases [2]. HGSOC is usually diagnosed at advanced stage and exhibits early peritoneal spread and lymph node metastasis, and resistance to conventional chemotherapy [3]. The development and molecular pathogenesis of HGSOC are largely unknown.

Approximately 50% of HGSOC cases were defective in homologous recombination (HR) DNA repair pathway. BRCA1/2 alterations, which can be derived from a combination of germline and somatic mutations, were seen in 22% of tumors [4]. Women with germline BRCA1/2 mutations have a 30–70%

chance of developing high-grade serous ovarian carcinoma by age 70 [5]. Poly (ADP-ribose) polymerase (PARP) is an abundant nuclear enzyme involved in repairing single-stand breaks in DNA [6]. Impaired homologous recombination (HR) DNA repair in cancer cells would render synthetic lethality with PARP1 inhibition [7]. Olaparib was the first PARP inhibitor approved in the European Union and the United States for the treatment of advanced BRCA-mutated ovarian cancer [8]. However, dysfunction of one DNA repair pathway may be compensated for by the function of another DNA damage response (DDR) pathway, which may be augmented and contribute to resistance to DNA-damaging chemotherapy and radiotherapy [9]. PARP inhibition in HR-deficient cells would result in increased activation of DNA-PK, increased nonhomologous end joining (NHEJ) activity [10]. High DNA-PKcs protein expression was associated with advanced stage and correlated with poor ovarian cancer specific survival [11]. Some of DNA repair pathways are upregulated in cancer and contribute to the progression of malignancy [9].

The Mre11-Rad50-Nbs1 (MRN) complex plays important roles in the detection and signaling of DNA double-strand breaks (DSBs), as well as the repair pathways of HR and NHEJ[12]. MRN complex acts as a double-strand break sensor for ATM and recruits ATM to broken DNA ends [13]. The role of the MRN complex in the response to DSBs as well as its requirement for cellular survival makes it a potential target for cancer therapy [14]. MRE11 promotes tumorigenesis by facilitating resistance to oncogene-induced replication stress [15]. Overexpression of NBS1 contributes to transformation through the activation of phosphatidylinositol 3-kinase/Akt [16].

Rad50, an ATPase, binds to Mre11 and Nbs1 to form a repair complex that is transported to the nucleus in response to DNA double-strand breaks [17]. mRad50 was essential for cellular viability and disruption of mRAD50 causes ES cell lethality, abnormal embryonic development and sensitivity to ionizing radiation [18]. Frequent lack of RAD50 was found in endometrial [19] and low-grade epithelial ovarian cancer [20]. Whereas Rad50 was highly expressed in melanoma [21] and gastric cancer [22]. High level of Rad50 was associated with poor prognosis in gastric and colorectal cancer [22, 23]. However, the expression pattern, functional role and clinical implication of Rad50 in HGSOC remain unclear.

In the present study, we found that oncogenic MYC directly transcriptionally activated Rad50 by binding its promoter. Upregulation of Rad50 is a frequent event in HGSOCs and enhanced Rad50 expression inversely correlated with patient survival. Furthermore, we elucidated that Rad50 overexpression promoted cell proliferation and invasiveness potentially via activation of the NFκB signaling pathway. Our findings indicate that MYC-regulated Rad50 may serve as a potential biomarker and therapeutic target for HGSOC.

Methods

Patients and tissue samples

This retrospective study included 151 cases of HGSOC and 33 cases of fallopian tube (FT) which were collected in Qilu hospital from November 2005 to December 2012. The HGSOC specimens were obtained

from primary ovarian cancer patients and the FT tissues were from patients suffered from other benign pathologic changes or uterine disease. All participants in this study gave written informed consent as delineated by the protocol which was approved by the Ethics Committee of Shandong University.

Tissue microarray construction and immunohistochemistry

Tissue microarrays (TMAs) were constructed according to the method described previously [24]. Immunohistochemistry (IHC) staining was performed on formalin-fixed paraffin-embedded HGSOC samples and xenograft tumors. Briefly, tissue slides were deparaffinized and rehydrated in a graded series of ethanol. After that, antigenic retrieval was proceeded by microwave heating. Nonspecific antigens were blocked with the 1.5% normal goat serum. Then they were incubated at 4 °C in a moist chamber overnight with antibodies against human Rad50 (1: 300, Abcam, Cambridge, MA, USA) and Ki67 (1:150, DAKO, Tokyo, Japan). The next day, the slides were incubated with the corresponding secondary antibody. The staining was detected with DAB detection system basing on the Biotin-Streptavidin HRP Detection Systems (Zhongshan Biotechnology Company, China). The final score of each sample was assessed by two independent pathologists based on intensity and extent of staining across the section. Staining intensity was graded according to the following standard: no staining (score 0); weak staining (score 1); moderate staining (score 2); strong staining (score 3). The proportion of every score was estimated for every sample as: 0 (0%), 1 (< 25%), 2 (25–50%), 3 (50–75%) and 4 (> 75%). The final staining index (SI) was calculated as the staining intensity score multiplied by the proportion of stained tumor cells. The cases were then divided into low ($SI \leq 6$) and high ($SI > 9$) groups.

Cell lines and cell culture

HO8910 cells were obtained from China Type Culture Collection (CTCC, Shanghai, China); A2780, SKOV3 and HEK293T cells were originally purchased from American Type Culture Collection (ATCC, VA, USA). HO8910 and A2780 cells were routinely cultured in RPMI-1640 medium (Gibco, NY, USA). SKOV3 cells were cultured in McCoy's 5A medium (Gibco, NY, USA) and HEK293T cells were cultured in DMEM (Gibco, NY, USA). All media were supplemented with 10% FBS (Gibco, NY, USA), 100 U/ml penicillin and 100 μg/ml streptomycin. All the cells were cultured at 37 °C, 5% CO_2 in a humidified incubator (Thermo Fisher Scientific, IL, USA).

Constructs and lentivirus infection

Rad50 overexpression and knockdown plasmids were obtained from Origene (Origene, MD, USA). Lentivirus was produced in HEK293T cells. For stable infection, 1×10^5 cells were plated in 6-well plates with 2 ml medium without antibiotics. After overnight incubation, the medium was replaced by 1 ml Opti-MEM Reduced-Serum Medium (Gibco, NY, USA) containing 50 μl of concentrated lentiviral particles and 8 μg/ml of polybrene per well. Fresh medium containing 2 μg/ml of puromycin (Invitrogen, USA) was added to each well 24 hours later and then selected for two weeks.

Western blot and immunoprecipitation

Western blot and immunoprecipitation were performed as described[25]. The primary antibodies included anti-Rad50 (Abcam, USA), anti-CARD9 (Protein Tech, USA), anti-p-p65 (Ser536), anti-p65, anti-$p21^{Cip1}$, anti-$p27^{Kip1}$, anti-Cyclin D1 (Cell Signaling Technology, USA),anti-MYC (Cell Signaling Technology, USA),anti-GAPDH(Zsbio, China) and anti-β-actin (Sigma-Aldrich, USA). Anti-E-cadherin, anti-N-cadherin, anti-Vimentin, anti-Twist and anti-Snail antibodies were all from the Epithelial-Mesenchymal Transition (EMT) Antibody Sampler Kit (Cell Signaling Technology, USA).

RNA isolation and real-time PCR

Total RNA from cells was extracted with TRIZOL reagent (Invitrogen, USA) according to the manufacturer's protocol. RNA was reverse transcripted to cDNA using PrimeScript RT reagent Kit (Takara, JAPAN). Real-time PCR was performed with SYBR Green mix and detected by the Bio-Rad CFX96. GAPDH was served as an endogenous control. Primer information was shown in Table S2.

Cellular proliferation assay

Cell proliferation was assessed by the 3-(4,5-dimethylthiazol-2-yl)-2,5-diphenyltetrazolium bromide (MTT, Sigma-Aldrich) assay. Cells were plated in 96-well plates ($2–3 \times 10^3$ per well) for continual 1–5 days. After incubation at designated times, 20 μl of MTT (5 mg/ml in PBS) was added to each well, and cells were incubated for another 4 h at 37 °C. The supernatants were carefully removed and 200 μl of dimethyl sulfoxide (DMSO, Sigma-Aldrich) was added to each well. The absorbance of each samples was measured at 490 nm with a Microplate Reader (Thermo Fisher Scientific, IL, USA).

Clonogenic assay

Cells were seeded into 6-well plates (300–500 cells/well) and cultured for 2–3 weeks. The colonies were fixed with methanol and stained with crystal violet. Colonies containing more than 50 cells were counted. For soft agar colony formation, $3–8 \times 10^3$ cells were suspended in the upper layer (0.7%) of the two layers agar (0.7 and 1.0%) in 6 cm dish. After 3 weeks, the colonies were stained by MTT and the images of colonies were photographed.

Cell cycle analysis

Cells ($2–3 \times 10^6$) were cultured overnight in medium without FBS. Then the cells were cultured in complete medium and harvested at different times. Cell suspensions were incubated with 1 ml PBS containing 50 μg/ml PI with RNase A and permeabilization buffer for 30 min. The DNA content was analyzed by flow cytometer with a FACScalibur (BD Biosciences, USA). The results were analyzed with the ModFit software (Becton-Dickinson, USA).

Invasion and migration assay

Invasion and migration assays were performed in 24-well transwell chambers (BD Biosciences, USA) system with 8 μm pores coated with or without diluted matrigel (BD Biosciences, USA). Briefly, $1.5\text{-}2 \times 10^5$ cells were seeded into the upper chambers in certain medium containing no FBS, and lower chambers were filled with culture media containing 10–20% FBS as a chemo-attractant. After incubating at 37 °C

for 12 to 48 h depending on the cell lines, cells that penetrated through the membrane were fixed with methanol and stained with crystal violet.

Immunofluorescence

Cells were seeded on sterile glass coverslips and cultured overnight at 37℃. Cells were washed with PBS and then fixed for 20 min with 4% paraformaldehyde. Following blocking with 10% goat serum in PBS for 2 h at room temperature, the cells were incubated with primary antibodies (anti-N-cadherin, anti-E-cadherin and anti-p65) overnight at 4℃. Cells were then incubated with Rhodamine/FITC-labeled secondary antibody (Beyotime Biotechnology, China) for 1 h at room temperature in the dark. Cells were washed with PBS three times before counterstaining with 1 μg/ml DAPI for 5 min in the dark. Finally, the slides were mounted with antifading reagent and examined with a fluorescence microscope (Olympus, Japan).

Chromatin immunoprecipitation (ChIP)

ChIP assay was conducted using EZ-Magna ChIP A/G Chromatin Immunoprecipitation Kit (Millipore) following manufacturer's instructions. Briefly, cells were cross-linked using formaldehyde. Then the cells were lysed and DNA was sheared to 200–500 bp fragments by sonication. The cell lysate was incubated with the Myc antibody (CST 9402S) and magnetic beads overnight at 4 °C with rotation. DNA associated with MYC is represented as fold change of normal IgG, calculated byΔCq method. Primer sequences were shown in Supplementary Table S1.

Luciferase assay

RAD50 wild type or truncated mutant promoter was cloned into pGL4.26 plasmid (Promega). Then RAD50 promotor report vector was co-transfected with pRL-TK and MYC plasmids into HEK293T cells. Luciferase activity was measured 24 hours after transfection using Dual-Luciferase Reporter Assay System (Promega) according to the manufacturer's protocol.

Xenograft tumor model

Female BALB/c nude mice (aged 4- 6weeks) were injected subcutaneously in bilateral flanks with cell suspensions (5×10^6 cells in 100 μl PBS). Tumor size was measured every three days after 1 week, and mice were killed with anesthesia after three weeks. Tumor volume was calculated according to the formula TV (cm^3) = $a \times b^2 \times \pi/6$, where 'a' is the longest diameter, and 'b' is the shortest diameter. Hematoxylin and eosin (H/E) staining and immunohistochemistry were performed on sections from embedded samples. All animal experiments were performed with the approval of Shandong University Animal Care and Use Committee.

Statistical analysis

The software GraphPad Prism 5 was used for statistical analysis. The two-tailed Student's t-test and one-way ANOVA analysis were used to analyze the differences. The relationship between the expression of

Rad50 and clinical pathological factors was analyzed by the chi-squared test. All error bars represent the standard error of three separate experiments. Differences with $P < 0.05$ were considered significant.

Results

MYC positively regulates Rad50 expression in high grade serous ovarian cancer

MYC is the most amplified gene (30–60%) of human ovarian tumors in the TCGA cohort [4]. Co-expression analysis showed that the mRNA expression of MYC was positively correlated with Rad50 as well as NBS1 and MRE11 (Fig. 1a and Fig. S1). To validate whether MYC regulates members of MRN complex, we knocked down MYC by siRNA in HEY and HO8910 cells. MYC depletion significantly downregulated expression of Rad50, NBS1 and MRE11 (Fig. 1b). In additional experiments, inhibition of MYC by JQ1 was observed to be markedly reduced the expression level of Rad50 and NBS1 in both cell lines (Fig. 1c). Rad50 was selected for further investigation since NBS1 was reported to be regulated by MYC previously[26]. Subsequently, we examined Rad50 expression by western blot and found forced MYC expression markedly enhanced protein level of Rad50 (Fig. 1d). Consistent with this, inhibition of MYC by siRNA or JQ1 reduced the protein level of Rad50 (Fig. 1d-e). These observations demonstrated that MYC positively regulates Rad50 expression in HGSOC.

MYC transcriptionally activates Rad50 through binding to its promoter

To determine whether MYC binds to the Rad50 promoter and transcriptionally regulates its expression. We analyzed Rad50 promoter region using JASPAR (http://jaspar.genereg.net/) and three putative MYC-binding sites were observed. Next, luciferase assay was performed and the result showed that forced expression of MYC increased luciferase activity of Rad50 promoter in SKOV3 and HO8910 cells (Fig. 2a). We further made truncated luciferase reporter vectors containing putative promoter region. Consistently, the luciferase activities of cells expressing truncated vectors were markedly lower than that of the full-length vector (Fig. 2b-c). Ectopic expression of MYC in HEK293T cells led to significant induction of the luciferase activity of truncated luciferase reporters containing putative MYC-binding sites respectively (Fig. 2d). Cistrome analysis showed MYC binding peaks was enriched in the promoter regions of Rad50 in multiple cell lines (Fig. 2e). Subsequently, ChIP assays in HEY cells demonstrated that MYC directly bound to promoter regions of Rad50 (Fig. 2f-g). Taken together, these data demonstrated that MYC transcriptionally activates Rad50 through binding to its promoter.

Rad50 is commonly elevated in HGSOCs and correlates with poor prognosis

To determine the expression and clinical significance of Rad50 in HGSOCs, we first examined Rad50 expression by western blot in HGSOCs and in fallopian tube (FT). As shown in Fig. 3a and Fig. S2a, Rad50 was overexpressed in a large proportion of the HGSOCs (n = 42) compared to FTs (n = 31). Consistently, immunohistochemical staining revealed a significant increase of Rad50 level in HGSOCs (n = 151) compared with FTs (n = 33) as illustrated in Fig. 3b. Furthermore, we analyzed clinicopathological and prognostic significance of Rad50 expression in HGSOCs (Table S1). Elevated Rad50 expression was correlated with lymph nodes metastasis ($P = 0.0410$) and the omentum metastasis ($P = 0.0362$). The association between Rad50 expression and overall survival was analyzed through Kaplan–Meier survival analysis of HGSOC patients. As shown in Fig. 3c-d, the high Rad50 level was significantly correlated with poor overall survival ($P = 0.0002$). Strikingly, Rad50 was upregulated in olaparib resistant ovarian cancer cells in GSE 117765 data (Fig. S2b). Taken together, these observations strongly indicate that Rad50 is commonly overexpressed and upregulation of Rad50 is associated with progression and poor prognosis in HGSOCs.

Ectopic expression of Rad50 promotes proliferation/invasion and induces epithelial-mesenchymal transition (EMT) of ovarian cancer cells

To explore the functional role of Rad50 in ovarian cancer, we established stable cell lines with Rad50 overexpression or knockdown (Fig. S2d). We then conducted clonogenic assay to evaluate the effect of Rad50 on the proliferation of ovarian cancer cells. Ectopic expression of Rad50 enhanced clonogenic capacity in HO8910 and A2780 cells while knockdown of Rad50 significantly reduced the colony-forming efficiency in A2780 and SKOV3 cells (Fig. 4a). We next performed soft agar colony formation assay and found Rad50 overexpression significantly increased whereas Rad50 knockdown reduced the colony number and the average colony size in soft agar (Fig. 4b). Moreover, Cell cycle analysis showed that Rad50 knockdown led to a decrease in the percentage of cells at S and G2-M phases compared with control group (Fig. S3a).

Because higher expression of Rad50 in HGSOC patients was associated with increased metastasis, we speculated that Rad50 may promote the invasiveness of ovarian cancer cells. We then measured migration and invasion abilities by transwell assay. Rad50 overexpression significantly enhanced the migration and invasion potential of A2780 and HO8910 cells while knockdown of Rad50 in A2780 and HO8910 cells led to reduced migration and invasion compared with control cells (Fig. 4c). Meanwhile, we found A2780 cells with Rad50 overexpression acquired more spindle-like morphology while Rad50 knockdown exhibited a more epithelial morphology compared to control cells (Fig. 4d). We further assessed the expression of EMT markers by Western blot and immunofluorescence. Ectopic expression of Rad50 in A2780 and HO8910 cells could obviously up-regulate mesenchymal phenotype markers (N-cadherin, Vimentin, Snail, Twist) and down-regulate epithelial phenotype marker (E-cadherin) while Rad50 knockdown upregulated epithelial marker and reduced the levels of mesenchymal markers in A2780 and SKOV3 cells (Fig. 4e and Fig. S4). Notably, knockdown of Rad50 in MYC-overexpressing cells attenuated

the promotion of ovarian cancer cell invasion and colony-forming efficiency (Fig. S5a-d). These findings suggest that Rad50 promotes migration /invasion and induces EMT in ovarian cancer cells.

Rad50 promotes tumor growth and metastasis of tumor xenografts

We next assessed the potential role of Rad50 on tumor growth and metastasis *in vivo*. Overexpression of Rad50 in A2780 cells significantly promoted ovarian tumor growth (Fig. 5a) whereas knockdown of Rad50 in SKOV3 cells remarkably reduced tumor burden in mice (Fig. 5b). Immunostaining of Ki-67 showed a higher proliferative index in tumors with Rad50 overexpression and a lower proliferative index in tumors with Rad50 knockdown than their corresponding control cells (Fig. 5c). We further evaluated metastasis-promoting potential of Rad50 in the lung metastasis model via tail vein injection and in the intraperitoneal metastatic model via intraperitoneal injection. As shown in Fig. 5d, knockdown of Rad50 in SKOV3 cells significantly reduced the number and size of lung metastasis nodules comparing with control. Meanwhile, overexpression of Rad50 in A2780 cells aggregated and formed much more dissemitated peritoneal tumors, while no peritoneal tumor was observed in the control group (Fig. S6). These results strongly suggest that Rad50 possesses potent oncogenic properties *in vivo*.

Rad50 induces aggressiveness in HGSOC via activation of NF-κB signaling pathway

A study on dendritic cells revealed that Rad50-CARD9 interaction activates NF-κB pathway when transfected with dsDNA or infected a DNA virus[27]. We then postulated that Rad50 may activate NF-κB pathway in ovarian cancer. We first examined the NF-κB pathway via immunoblot. Interestingly, overexpression of Rad50 increased the phosphorylation of p65 and decreased total IκBα protein levels while knockdown of Rad50 significantly decreased p-p65 protein level in ovarian cancer cell lines (Fig. 6a). We further examined the nuclear localization of p65 protein by Western blot of fractionated proteins and found levels of the activated nuclear form p-p65 were significantly higher in A2780 cells with Rad50 overexpression compared to control cells (Fig. 6b, left panel). While knockdown of Rad50 inhibited the translocation of p-p65 to the nucleus in both A2780 and SKOV3 cell lines (Fig. 6b, middle and right panels). Immunofluorescence data showed that ectopic expression of Rad50 induced, whereas downregulation of Rad50 inhibited nuclear localization of p-p65 (Fig. 6c). To determine whether Rad50 drives the HGSOC aggressive behavior through NF-κB activation, we blocked the NF-κB pathway by PDTC in Rad50-overexpressing cells. As expected, PDTC treatment decreased Rad50-induced invasiveness and EMT (Fig. 6d and Fig. S7a). These results suggest that Rad50 activates NF-κB and the oncogenic function of Rad50 is dependent on the activation of NF-κB.

We proposed that Rad50 may also activate NF-κB pathway via the interaction with CARD9 in ovarian cancer cells. To this end, we performed immunoprecipitation (IP) –western blot to test whether Rad50 can interact with CARD9 in ovarian cancer cells. As indicated in Fig. 6e, CARD9 was detected in the immunoprecipitates with anti-Rad50 antibody, but not with the control mouse IgG in HEK293T and

ovarian cancer cell lines. Consistently, Rad50 was detected in the immunoprecipitates with anti-CARD9 antibody (Fig. 6e). To verify whether Rad50-mediated activation of NF-κB pathway is CARD9 dependent, we knocked down CARD9 in Rad50-overexpressed ovarian cancer cell lines and found knockdown of CARD9 significantly reversed Rad50-induced migration activities (Fig. S7b). Consistent with this, activated nuclear form p-p65 induced by Rad50 was attenuated by siRNAs targeting CARD9 (Fig. S7b). Therefore, we identified CARD9 as an interacting protein of Rad50 in ovarian cancer cells and Rad50-mediated activation of NF-κB pathway is CARD9 dependent. The diagram of the mechanism that MYC targeted Rad50 drives ovarian cancer progression via NF-κB activation was presented in Fig. 7.

Discussion

DDR is a double-edged sword in cancer prevention and cancer therapy. It acts as a positive guardian of genomic stability to prevent tumorigenesis. On the other hand, DDR also functions as a negative saboteur to resist chemo- and radiotherapy [28]. In our study, we reported that MYC proto-oncogene transcriptionally activated Rad50 expression in high-grade serous ovarian cancer. Rad50 was commonly upregulated in HGSOC and enhanced Rad50 expression inversely correlated with patient survival and metastasis. In agreement with our results, previous studies also reported that high expression of Rad50 were associated with poor prognosis in lung [29] and gastric [22] cancer.

In addition to conferring chemoresistance and radioresistance, high expression of DNA repair genes has been shown to exhibit oncogenic properties. Overexpression of Ku proteins promotes oncogenic phenotypes, including hyperproliferation and resistance to apoptosis [30]. DNA-PKcs drives prostate cancer progression and metastasis via transcriptional regulation [31]. MRE11 promotes cell proliferation, tumor invasion, and DNA repair in breast cancer [32]. Increased NBS1 expression is a marker of aggressive head and neck cancer and overexpression of NBS1 contributes to transformation [33]. PARP1, which is overexpressed in ovarian cancer, was shown to promote cancer cell survival by repressing the expression of NOX 1 and NOX4 [34]. Our findings in this study demonstrated that Rad50 has oncogenic properties in ovarian cancer. These studies expanded our understanding of the functions of DNA repair genes in tumorigenesis.

Although Rad50-CARD9 interaction activates NF-κB pathway has been reported in dendritic cells [27], we demonstrated that Rad50-CARD9 interaction activates NF-κB pathway in ovarian cancer cells. Overexpression of Rad50 increased the phosphorylation of p65 and decreased total IκBα protein levels while knockdown of Rad50 significantly decreased p-p65 protein level in ovarian cancer cell lines. PDTC treatment decreased Rad50-induced invasiveness and EMT. Furthermore, we verified CARD9 as a specific interacting protein of Rad50 in ovarian cancer cells and Rad50-mediated activation of NF-κB pathway is CARD9 dependent. Many human cancers, including ovarian cancer, possess high levels of constitutive NF-κB activity [35]. CARD9 contributes to tumor metastasis by promoting metastasis-associated macrophage polarization through activation of the NF-κB signaling pathway [36]. Thus, it is possible that ectopic expression of Rad50 may recruit CARD9 and contribute to tumor metastasis through activating

NF-κB pathway in HGSOC. Future studies will be required to explore the molecular cooperation between Rad50 and CARD9 in promoting proliferation/invasion and induces EMT in ovarian cancer.

Conclusions

Our findings showed that MYC-regulated Rad50 exhibits oncogenic property in ovarian cancer. We provided evidence that Rad50 ectopic expression promotes migration /invasion and induces EMT in ovarian cancer cells. Rad50 induces aggressiveness in HGSOC via activation NF-κB signaling pathway. Our data suggest that Rad50 could be a prognostic biomarker and potential therapeutic target for ovarian cancer.

Abbreviations

HGSOC: High-grade serous ovarian carcinoma; TCGA: The Cancer Genome Atlas; DSBs: Double-strand breaks; IHC: Immunohistochemistry; qPCR: Real-time quantitative PCR

MRN: Mre11-Rad50-Nbs1; HR: homologous recombination

Declarations

Ethics approval and consent to participate

All procedures involving animals were approved by the ethics committee of Shandong University. All participants in this study gave written informed consent as delineated by the protocol which was approved by the Ethics Committee of Shandong University.

Consent for publication

Not applicable

Availability of data and materials

Not applicable

Competing interests

No potential conflicts of interest were disclosed.

Funding

This work was supported by National Natural Science Foundation of China (81972437, 81672578), and Key Research and Development Program of Shandong Province (2019GSF108122).

Author contributions

Conception and design: Beihua Kong; Zhaojian Liu. Development and methodology:Yinuo Li; Shourong Wang; Peng Li. Acquisition of data: Yinuo Li; Shourong Wang; Yao Liu; Haiya Fang. Analysis and interpretation of data: Yinuo Li; Shourong Wang. Administrative, technical, or material support: Zhaojian Liu; Xiyu Zhang; Haiya Fang. Study supervision: Beihua Kong; Zhaojian Liu. Writing, review, and/or revision of the manuscript: All authors. Final approval: All authors.

Acknowledgements

We thank Translational Medicine Core Facility of Shandong University for consultation and instrument availability that supported this work.

References

1. Bast RC, Jr., Hennessy B, Mills GB: The biology of ovarian cancer: new opportunities for translation. Nat Rev Cancer 2009, 9:415-428.
2. Chen C, Gupta P, Parashar D, Nair GG, George J, Geethadevi A, et al: ERBB3-induced furin promotes the progression and metastasis of ovarian cancer via the IGF1R/STAT3 signaling axis. Oncogene 2020.
3. Meng J, Liu K, Shao Y, Feng X, Ji Z, Chang B, Wang Y, Xu L, Yang G: ID1 confers cancer cell chemoresistance through STAT3/ATF6-mediated induction of autophagy. Cell Death Dis 2020, 11:137.
4. Cancer Genome Atlas Research N: Integrated genomic analyses of ovarian carcinoma. Nature 2011, 474:609-615.
5. Liu Z, Liu J, Segura MF, Shao C, Lee P, Gong Y, Hernando E, Wei JJ: MiR-182 overexpression in tumourigenesis of high-grade serous ovarian carcinoma. J Pathol 2012, 228:204-215.
6. Mullard A: PARP inhibitor pick-me-up. Nat Rev Drug Discov 2019, 18:814.
7. Zimmermann M, Murina O, Reijns MAM, Agathanggelou A, Challis R, Tarnauskaite Z, et al: CRISPR screens identify genomic ribonucleotides as a source of PARP-trapping lesions. Nature 2018, 559:285-289.
8. Mateo J, Lord CJ, Serra V, Tutt A, Balmana J, Castroviejo-Bermejo M, Cruz C, Oaknin A, Kaye SB, de Bono JS: A decade of clinical development of PARP inhibitors in perspective. Ann Oncol 2019, 30:1437-1447.
9. Curtin NJ: DNA repair dysregulation from cancer driver to therapeutic target. Nat Rev Cancer 2012, 12:801-817.
10. Fok JHL, Ramos-Montoya A, Vazquez-Chantada M, Wijnhoven PWG, Follia V, James N, et al: AZD7648 is a potent and selective DNA-PK inhibitor that enhances radiation, chemotherapy and olaparib activity. Nat Commun 2019, 10:5065.
11. Abdel-Fatah TM, Arora A, Moseley P, Coveney C, Perry C, Johnson K, Kent C, Ball G, Chan S, Madhusudan S: ATM, ATR and DNA-PKcs expressions correlate to adverse clinical outcomes in

epithelial ovarian cancers. BBA Clin 2014, 2:10-17.

12. Stingele J, Bellelli R, Boulton SJ: Mechanisms of DNA-protein crosslink repair. Nat Rev Mol Cell Biol 2017, 18:563-573.
13. Cassani C, Vertemara J, Bassani M, Marsella A, Tisi R, Zampella G, Longhese MP: The ATP-bound conformation of the Mre11-Rad50 complex is essential for Tel1/ATM activation. Nucleic Acids Res 2019, 47:3550-3567.
14. Chang L, Huang J, Wang K, Li J, Yan R, Zhu L, Ye J, Wu X, Zhuang S, Li D, Zhang G: Targeting Rad50 sensitizes human nasopharyngeal carcinoma cells to radiotherapy. BMC Cancer 2016, 16:190.
15. Spehalski E, Capper KM, Smith CJ, Morgan MJ, Dinkelmann M, Buis J, Sekiguchi JM, Ferguson DO: MRE11 Promotes Tumorigenesis by Facilitating Resistance to Oncogene-Induced Replication Stress. Cancer Res 2017, 77:5327-5338.
16. Chen YC, Su YN, Chou PC, Chiang WC, Chang MC, Wang LS, Teng SC, Wu KJ: Overexpression of NBS1 contributes to transformation through the activation of phosphatidylinositol 3-kinase/Akt. J Biol Chem 2005, 280:32505-32511.
17. Bai Y, Wang W, Li S, Zhan J, Li H, Zhao M, et al: C1QBP Promotes Homologous Recombination by Stabilizing MRE11 and Controlling the Assembly and Activation of MRE11/RAD50/NBS1 Complex. Mol Cell 2019, 75:1299-1314 e1296.
18. Luo G, Yao MS, Bender CF, Mills M, Bladl AR, Bradley A, Petrini JH: Disruption of mRad50 causes embryonic stem cell lethality, abnormal embryonic development, and sensitivity to ionizing radiation. Proc Natl Acad Sci U S A 1999, 96:7376-7381.
19. Koppensteiner R, Samartzis EP, Noske A, von Teichman A, Dedes I, Gwerder M, et al: Effect of MRE11 loss on PARP-inhibitor sensitivity in endometrial cancer in vitro. PLoS One 2014, 9:e100041.
20. Brandt S, Samartzis EP, Zimmermann AK, Fink D, Moch H, Noske A, Dedes KJ: Lack of MRE11-RAD50-NBS1 (MRN) complex detection occurs frequently in low-grade epithelial ovarian cancer. BMC Cancer 2017, 17:44.
21. Avaritt NL, Owens R, Larson SK, Reynolds M, Byrum S, Hiatt KM, Smoller BR, Tackett AJ, Cheung WL: Misregulation of Rad50 expression in melanoma cells. J Cutan Pathol 2012, 39:680-684.
22. Altan B, Yokobori T, Ide M, Bai T, Yanoma T, Kimura A, et al: High Expression of MRE11-RAD50-NBS1 Is Associated with Poor Prognosis and Chemoresistance in Gastric Cancer. Anticancer Res 2016, 36:5237-5247.
23. Chen C, Wang Y, Mei JF, Li SS, Xu HX, Xiong HP, Wang XH, He X: Targeting RAD50 increases sensitivity to radiotherapy in colorectal cancer cells. Neoplasma 2018, 65:75-80.
24. Kononen J, Bubendorf L, Kallioniemi A, Barlund M, Schraml P, Leighton S, Torhorst J, Mihatsch MJ, Sauter G, Kallioniemi OP: Tissue microarrays for high-throughput molecular profiling of tumor specimens. Nat Med 1998, 4:844-847.
25. Lin Z, Tan C, Qiu Q, Kong S, Yang H, Zhao F, et al: Ubiquitin-specific protease 22 is a deubiquitinase of CCNB1. Cell Discov 2015, 1.

26. Chiang YC, Teng SC, Su YN, Hsieh FJ, Wu KJ: c-Myc directly regulates the transcription of the NBS1 gene involved in DNA double-strand break repair. J Biol Chem 2003, 278:19286-19291.
27. Roth S, Rottach A, Lotz-Havla AS, Laux V, Muschaweckh A, Gersting SW, et al: Rad50-CARD9 interactions link cytosolic DNA sensing to IL-1beta production. Nat Immunol 2014, 15:538-545.
28. Tian H, Gao Z, Li H, Zhang B, Wang G, Zhang Q, Pei D, Zheng J: DNA damage response--a double-edged sword in cancer prevention and cancer therapy. Cancer Lett 2015, 358:8-16.
29. Wang Y, Gudikote J, Giri U, Yan J, Deng W, Ye R, et al: RAD50 Expression Is Associated with Poor Clinical Outcomes after Radiotherapy for Resected Non-small Cell Lung Cancer. Clin Cancer Res 2018, 24:341-350.
30. Gullo C, Au M, Feng G, Teoh G: The biology of Ku and its potential oncogenic role in cancer. Biochim Biophys Acta 2006, 1765:223-234.
31. Goodwin JF, Kothari V, Drake JM, Zhao S, Dylgjeri E, Dean JL, et al: DNA-PKcs-Mediated Transcriptional Regulation Drives Prostate Cancer Progression and Metastasis. Cancer Cell 2015, 28:97-113.
32. Yuan SS, Hou MF, Hsieh YC, Huang CY, Lee YC, Chen YJ, Lo S: Role of MRE11 in cell proliferation, tumor invasion, and DNA repair in breast cancer. J Natl Cancer Inst 2012, 104:1485-1502.
33. Yang MH, Chiang WC, Chou TY, Chang SY, Chen PM, Teng SC, Wu KJ: Increased NBS1 expression is a marker of aggressive head and neck cancer and overexpression of NBS1 contributes to transformation. Clin Cancer Res 2006, 12:507-515.
34. Hou D, Liu Z, Xu X, Liu Q, Zhang X, Kong B, Wei JJ, Gong Y, Shao C: Increased oxidative stress mediates the antitumor effect of PARP inhibition in ovarian cancer. Redox Biol 2018, 17:99-111.
35. Baldwin AS, Jr.: The NF-kappa B and I kappa B proteins: new discoveries and insights. Annu Rev Immunol 1996, 14:649-683.
36. Yang M, Shao JH, Miao YJ, Cui W, Qi YF, Han JH, Lin X, Du J: Tumor cell-activated CARD9 signaling contributes to metastasis-associated macrophage polarization. Cell Death Differ 2014, 21:1290-1302.

Figures

Figure 1

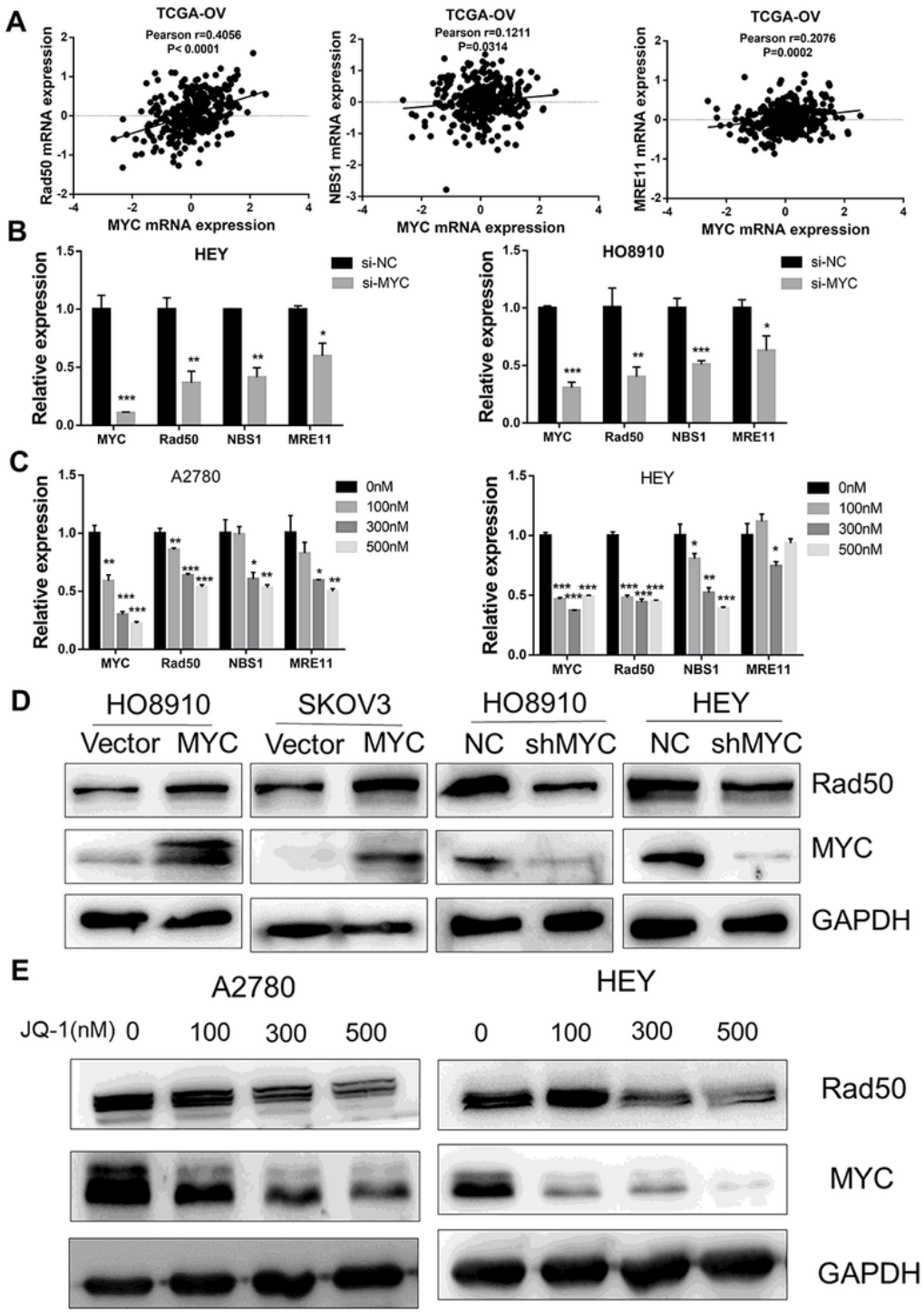

Figure 1

MYC positively regulates Rad50 expression in high grade serous ovarian cancer. a Correlation analysis of mRNA expression between MYC and Rad50, NBS1, MRE11 was conducted in TCGA ovarian cancer cohort. b-c MYC, Rad50, NBS1 and MRE11 expression was measured by qPCR after MYC knocked down or treated with JQ-1. d Western blot analysis of MYC and Rad50 protein level after MYC overexpression or knockdown in ovarian cancer cells. e Western blot analysis of MYC and Rad50 protein level in ovarian

cancer cells treated with different concentration of JQ-1. *P < 0.05, **P<0.01, ***P<0.001, when compared with control group.

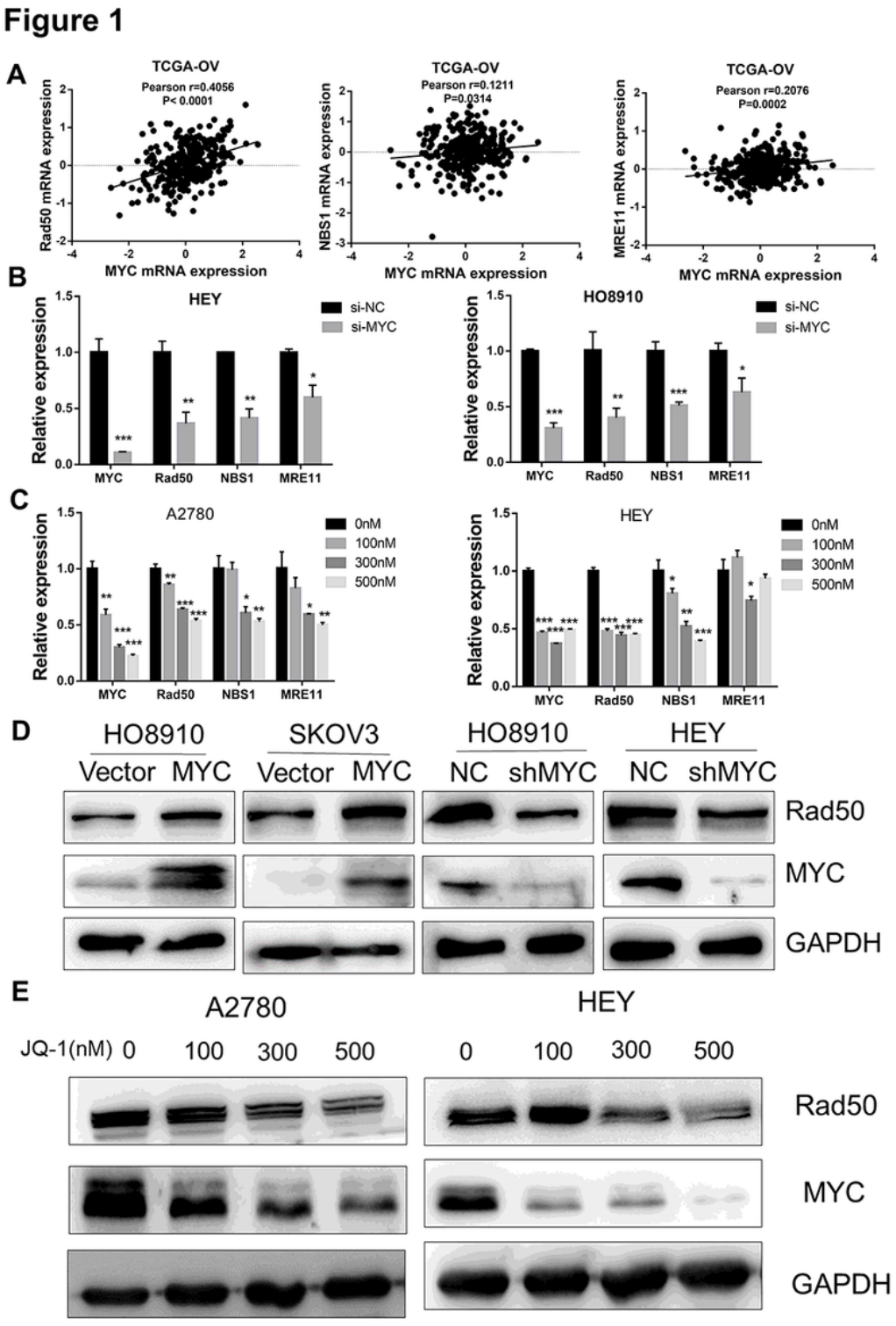

Figure 1

MYC positively regulates Rad50 expression in high grade serous ovarian cancer. a Correlation analysis of mRNA expression between MYC and Rad50, NBS1, MRE11 was conducted in TCGA ovarian cancer cohort. b-c MYC, Rad50, NBS1 and MRE11 expression was measured by qPCR after MYC knocked down

or treated with JQ-1. d Western blot analysis of MYC and Rad50 protein level after MYC overexpression or knockdown in ovarian cancer cells. e Western blot analysis of MYC and Rad50 protein level in ovarian cancer cells treated with different concentration of JQ-1. *P < 0.05, **P<0.01, ***P<0.001, when compared with control group.

Figure 1

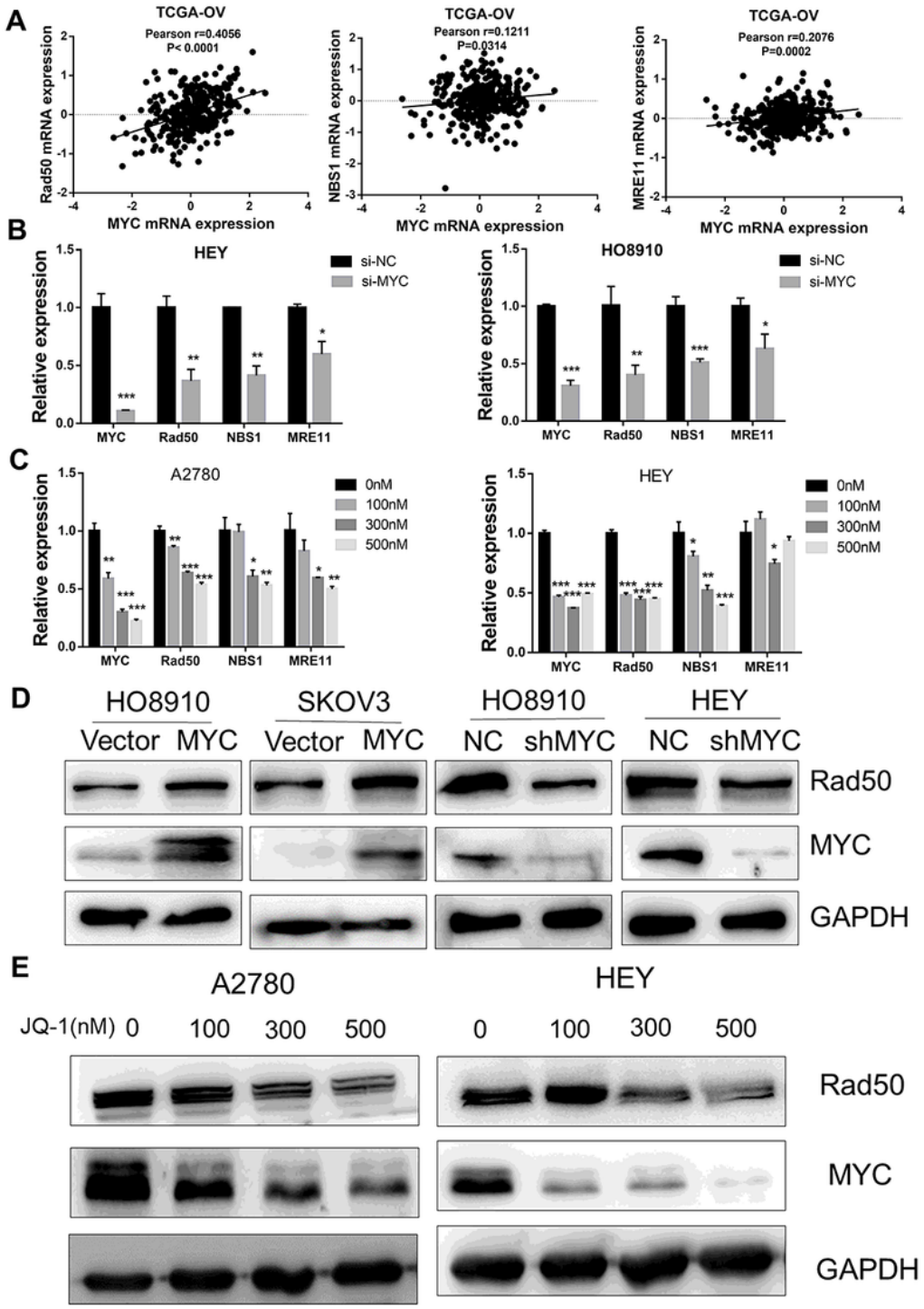

Figure 1

MYC positively regulates Rad50 expression in high grade serous ovarian cancer. a Correlation analysis of mRNA expression between MYC and Rad50, NBS1, MRE11 was conducted in TCGA ovarian cancer cohort. b-c MYC, Rad50, NBS1 and MRE11 expression was measured by qPCR after MYC knocked down or treated with JQ-1. d Western blot analysis of MYC and Rad50 protein level after MYC overexpression or knockdown in ovarian cancer cells. e Western blot analysis of MYC and Rad50 protein level in ovarian cancer cells treated with different concentration of JQ-1. *P < 0.05, **P<0.01, ***P<0.001, when compared with control group.

Figure 2

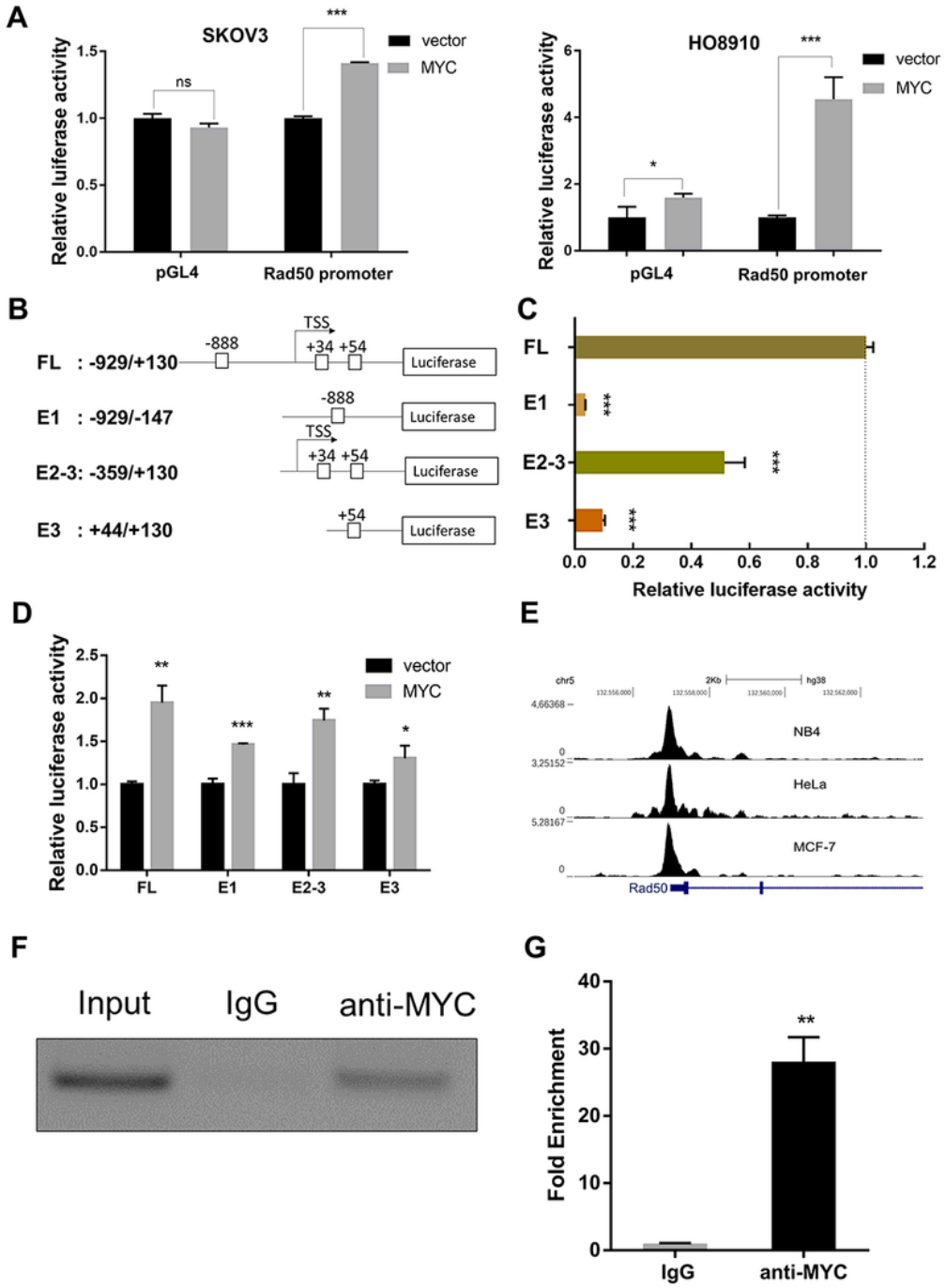

Figure 2

MYC transcriptionally activates Rad50 through binding to its promoter. a luciferase activity was measured in SKOV3 and HO8910 cells cotransfected with MYC and pGL4 plasmids containing with or without Rad50 promoter. b-c luciferase activity was measured in HEK293T cells transfected with pGL4 plasmids containing full length or truncated Rad50 promoters. d Luciferase activity was measured in HEK293T cells co-transfected MYC and pGL4 plasmids containing full length or truncated Rad50 promoters. e MYC binding peaks on Rad50 promoter region were shown in different cell lines based on ChIP-seq data in UCSC genome browser. f-g ChIP assays were performed in HEK293T cells and the binding of MYC on Rad50 promoter was measured by PCR. *P < 0.05, **P<0.01, ***P<0.001, when compared with control group.

Figure 2

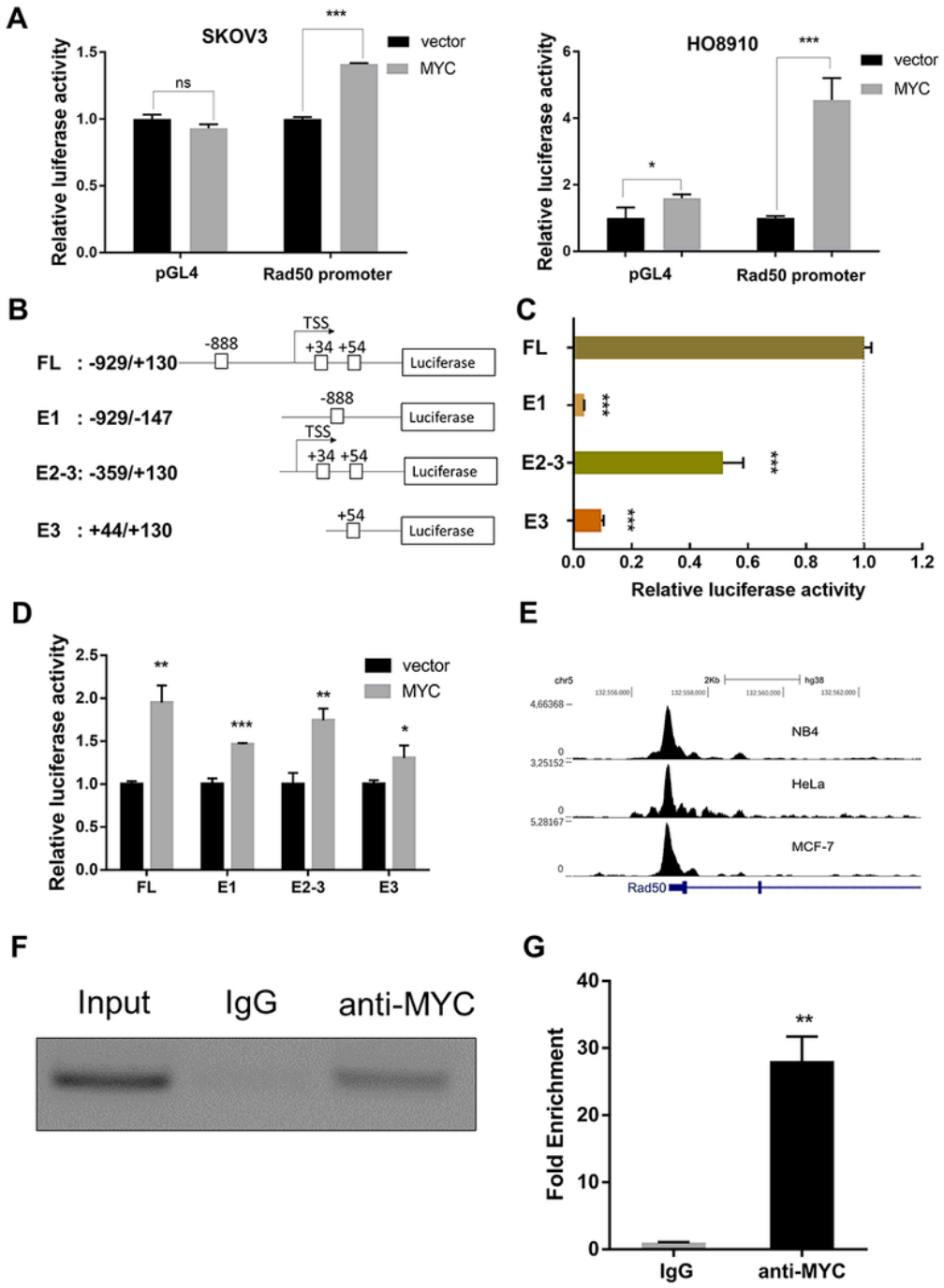

Figure 2

MYC transcriptionally activates Rad50 through binding to its promoter. a luciferase activity was measured in SKOV3 and HO8910 cells cotransfected with MYC and pGL4 plasmids containing with or without Rad50 promoter. b-c luciferase activity was measured in HEK293T cells transfected with pGL4 plasmids containing full length or truncated Rad50 promoters. d Luciferase activity was measured in HEK293T cells co-transfected MYC and pGL4 plasmids containing full length or truncated Rad50

promoters. e MYC binding peaks on Rad50 promoter region were shown in different cell lines based on ChIP-seq data in UCSC genome browser. f-g ChIP assays were performed in HEK293T cells and the binding of MYC on Rad50 promoter was measured by PCR. *P < 0.05, **P<0.01, ***P<0.001, when compared with control group.

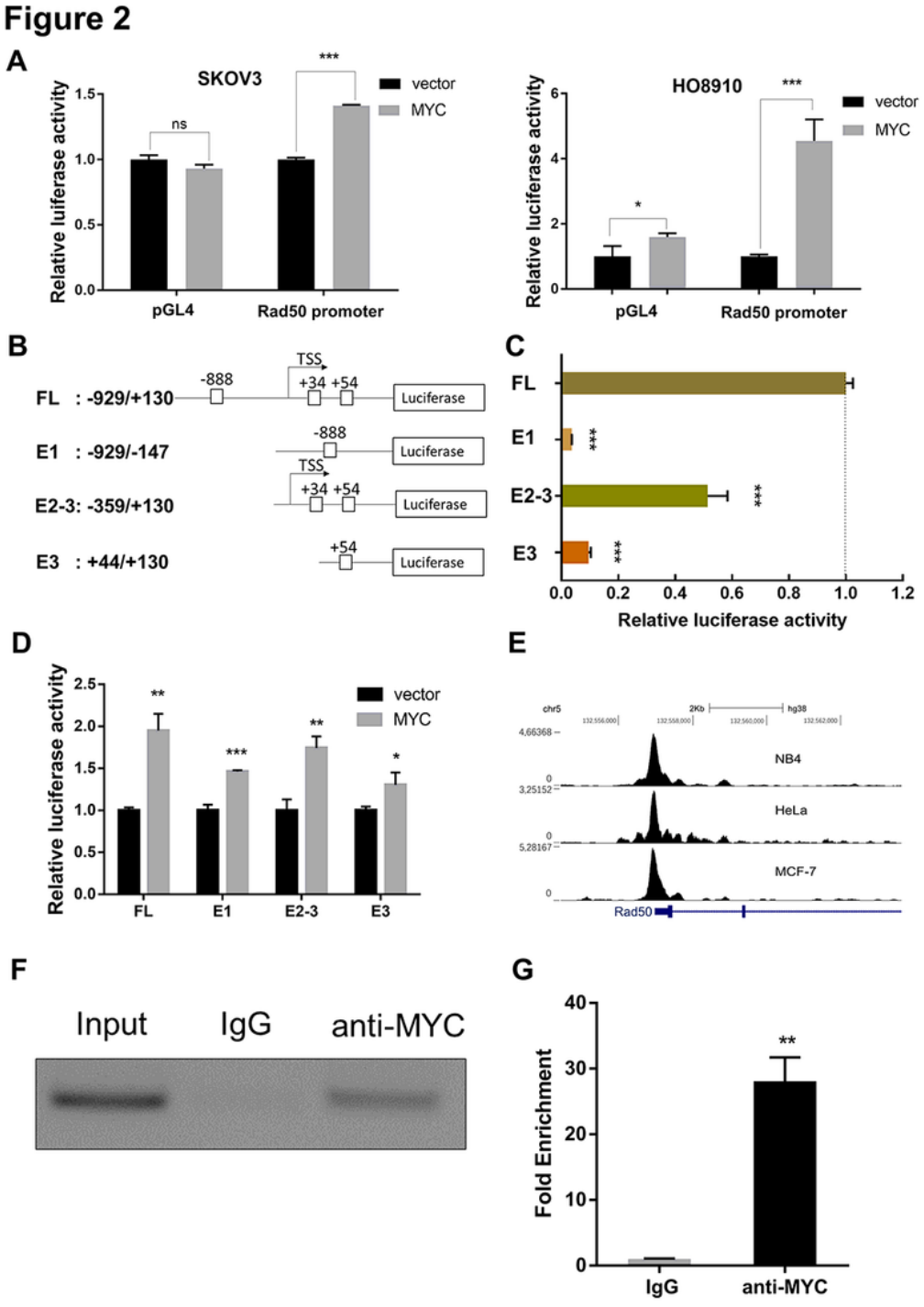

Figure 2

MYC transcriptionally activates Rad50 through binding to its promoter. a luciferase activity was measured in SKOV3 and HO8910 cells cotransfected with MYC and pGL4 plasmids containing with or without Rad50 promoter. b-c luciferase activity was measured in HEK293T cells transfected with pGL4 plasmids containing full length or truncated Rad50 promoters. d Luciferase activity was measured in HEK293T cells co-transfected MYC and pGL4 plasmids containing full length or truncated Rad50 promoters. e MYC binding peaks on Rad50 promoter region were shown in different cell lines based on ChIP-seq data in UCSC genome browser. f-g ChIP assays were performed in HEK293T cells and the binding of MYC on Rad50 promoter was measured by PCR. *P < 0.05, **P<0.01, ***P<0.001, when compared with control group.

Figure 3

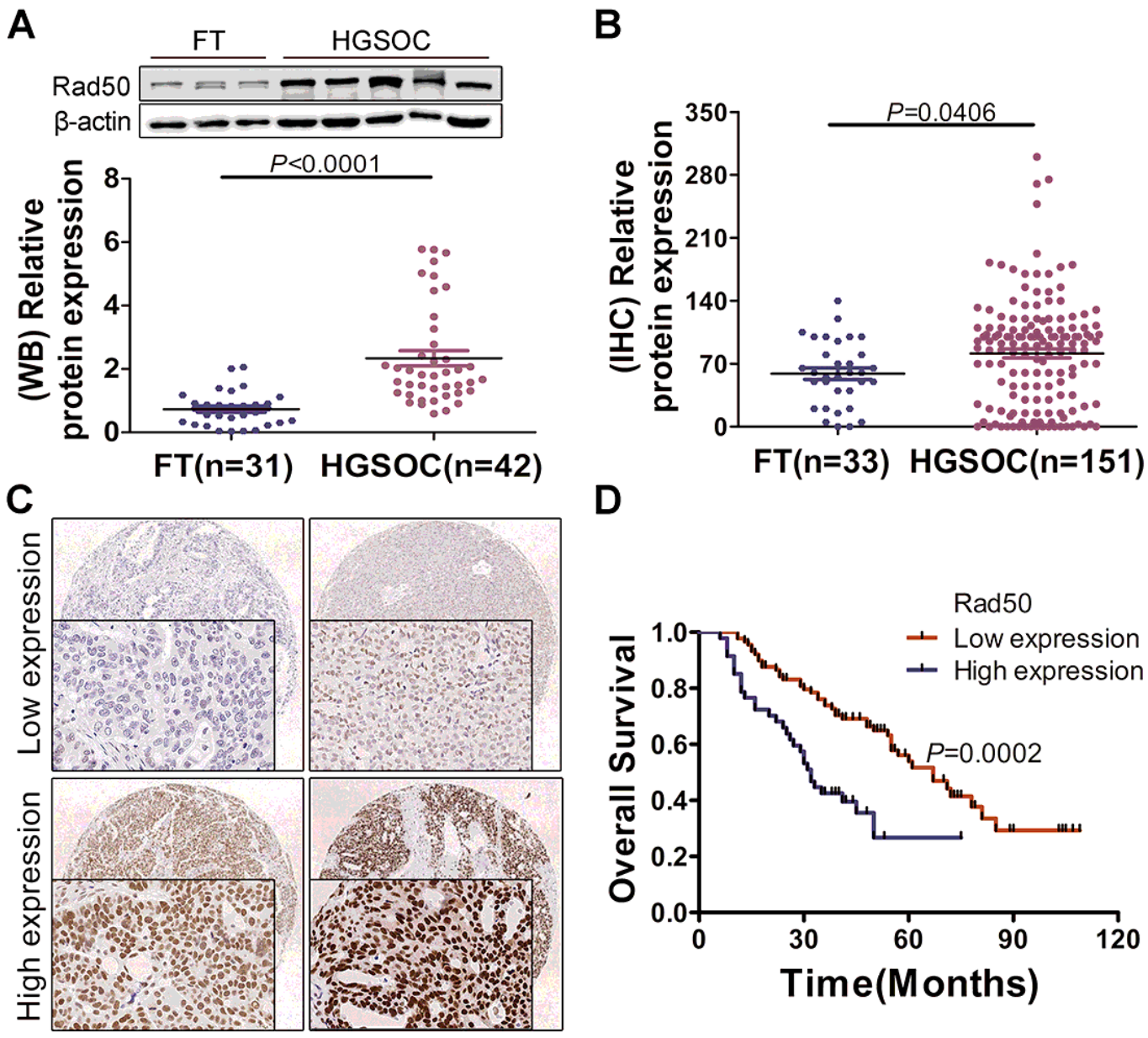

Figure 3

Rad50 is commonly elevated in HGSOCs and correlates with poor prognosis. a Western blot analysis of Rad50 in HGSOC (n=42) compared to normal fimbria (n=31). b The plot graph reveals the statistical result of Rad50 expression in HGSOC (n=151) compared to normal fimbria (n=33) assessed by IHC. c Representative images of immunohistochemical staining of Rad50 in the tissue microarray. d Kaplan–Meier plots of overall survival for HGSOC patients dichotomized based on low (Score ≤6) versus high (Score >6) Rad50 IHC expression level (P=0.0002).

Figure 3

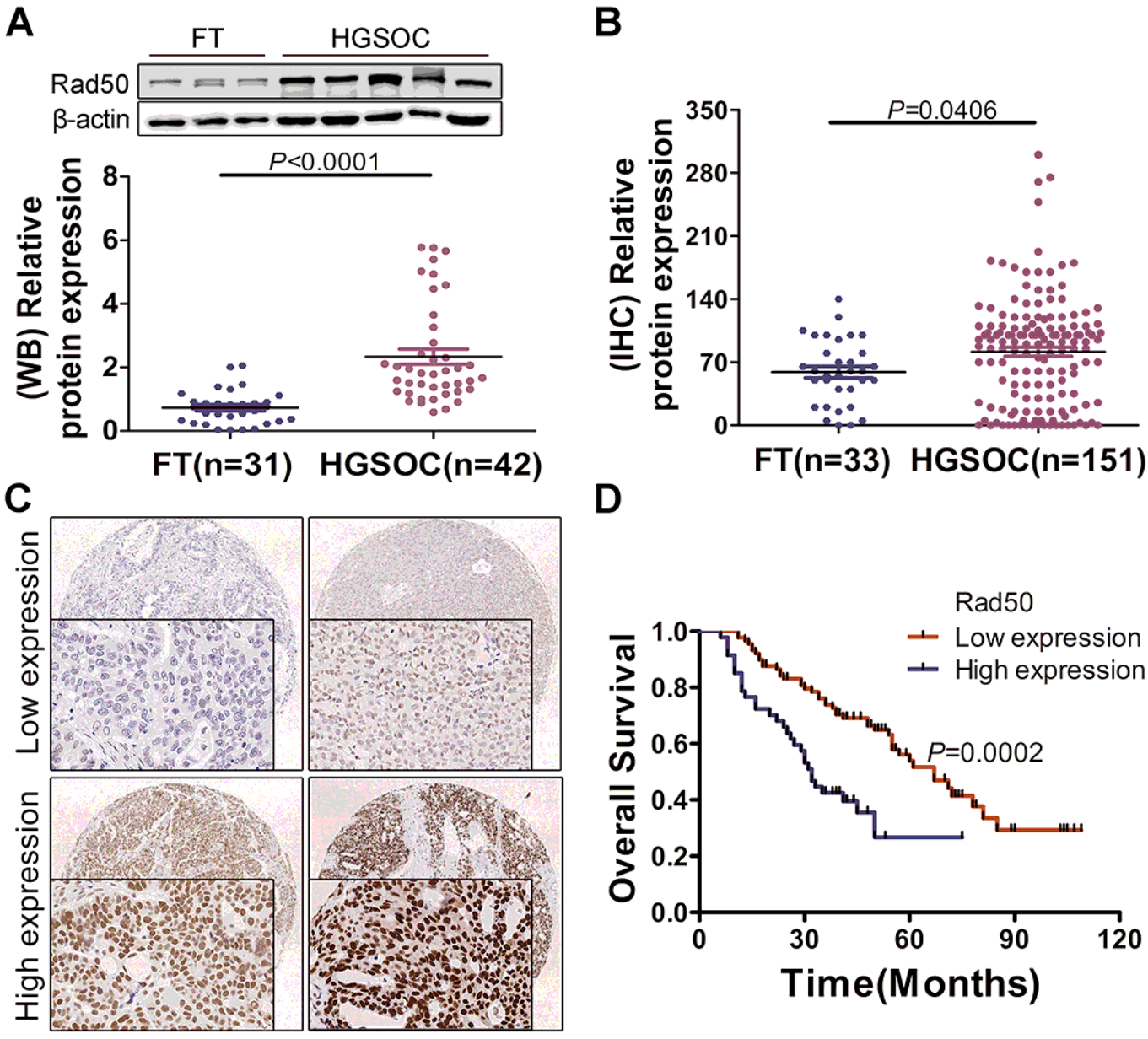

Figure 3

Rad50 is commonly elevated in HGSOCs and correlates with poor prognosis. a Western blot analysis of Rad50 in HGSOC (n=42) compared to normal fimbria (n=31). b The plot graph reveals the statistical result of Rad50 expression in HGSOC (n=151) compared to normal fimbria (n=33) assessed by IHC. c

Representative images of immunohistochemical staining of Rad50 in the tissue microarray. d Kaplan–Meier plots of overall survival for HGSOC patients dichotomized based on low (Score ≤6) versus high (Score >6) Rad50 IHC expression level (P=0.0002).

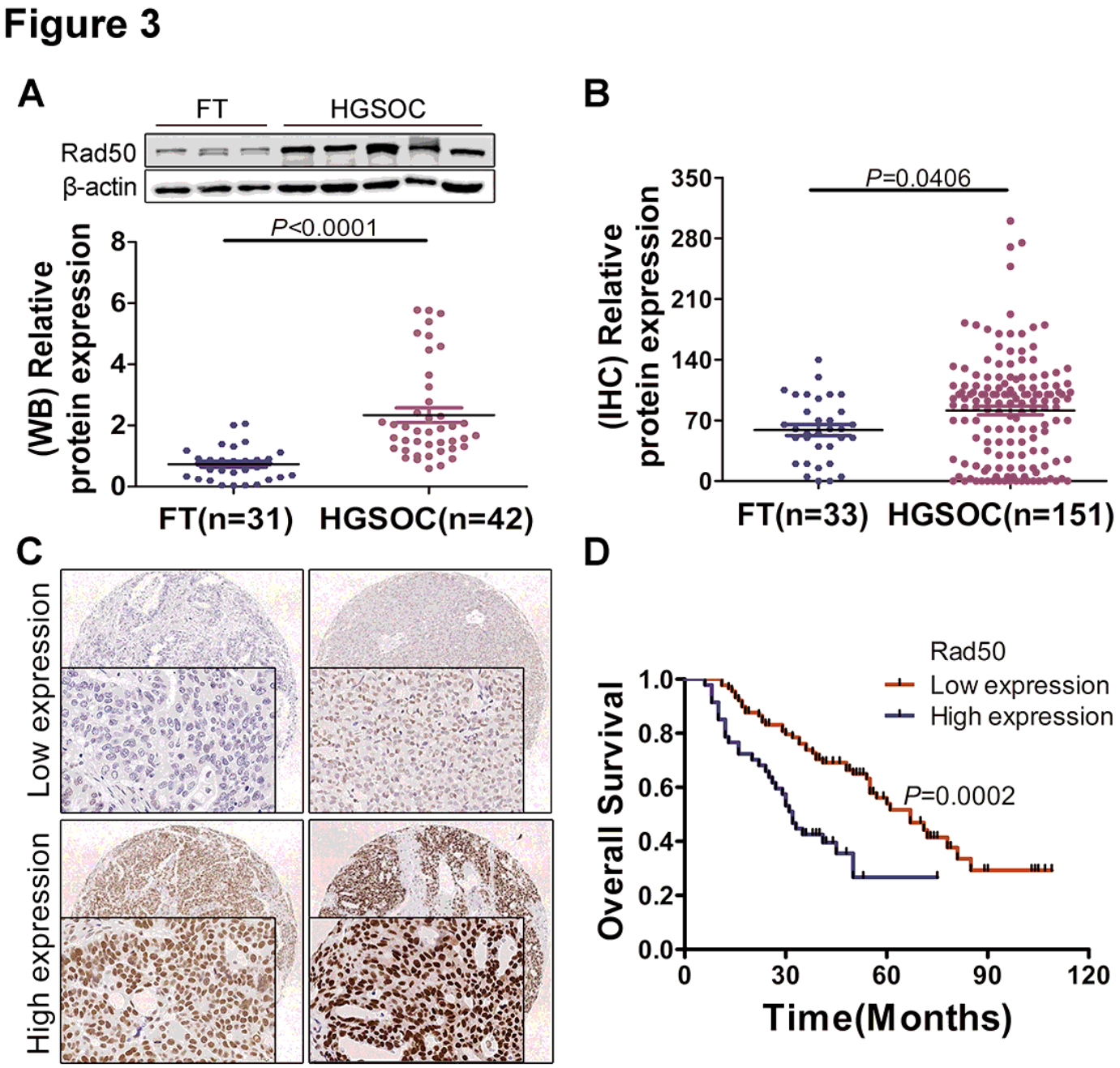

Figure 3

Rad50 is commonly elevated in HGSOCs and correlates with poor prognosis. a Western blot analysis of Rad50 in HGSOC (n=42) compared to normal fimbria (n=31). b The plot graph reveals the statistical result of Rad50 expression in HGSOC (n=151) compared to normal fimbria (n=33) assessed by IHC. c Representative images of immunohistochemical staining of Rad50 in the tissue microarray. d Kaplan–Meier plots of overall survival for HGSOC patients dichotomized based on low (Score ≤6) versus high (Score >6) Rad50 IHC expression level (P=0.0002).

Figure 4

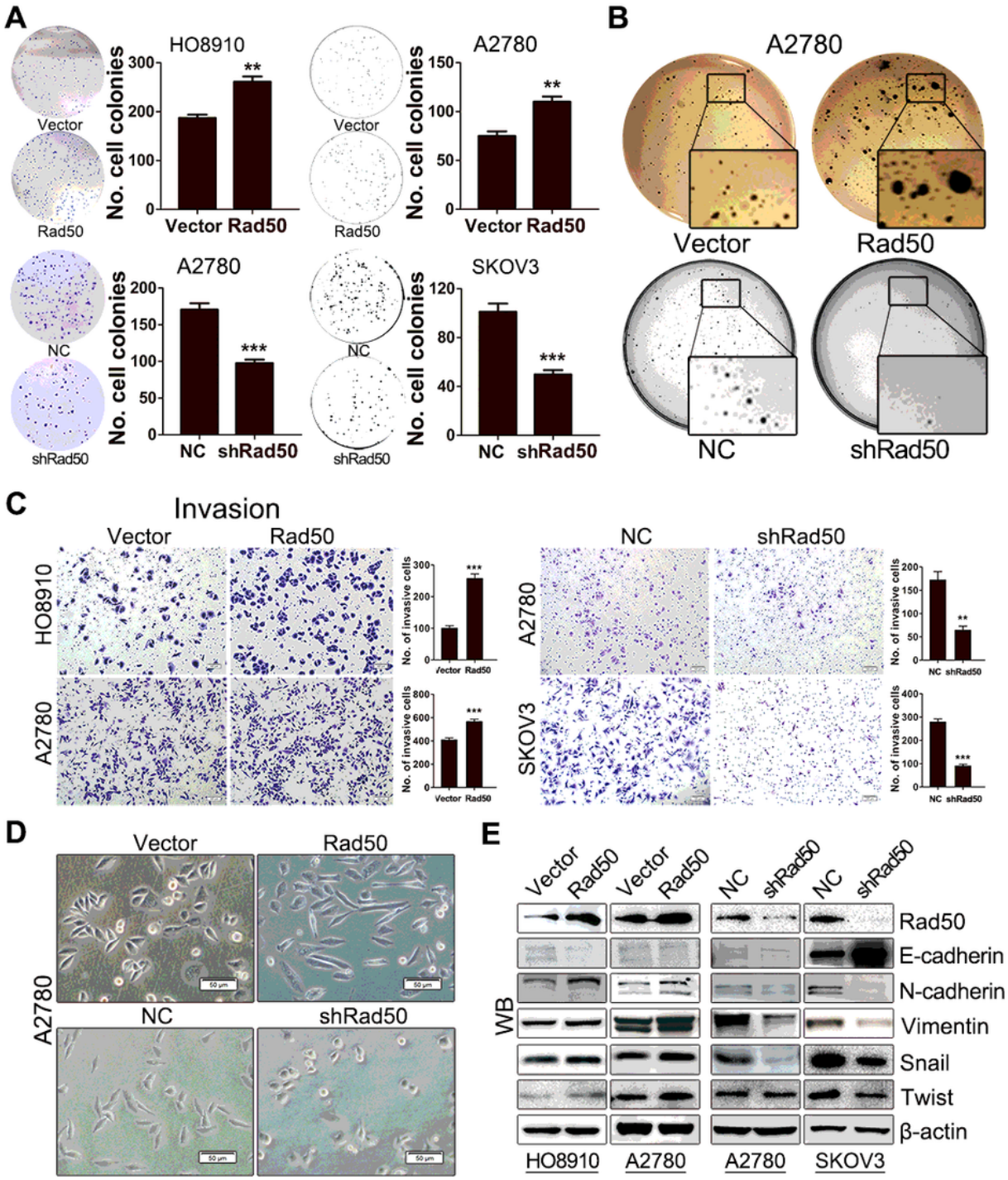

Figure 4

Rad50 promotes proliferation and invasion of ovarian cancer cells. a Effect of Rad50 on clonogenic ability in ovarian cancer cell lines. b Soft agar colony formation assay exhibited the effect of Rad50 on anchorage-independent growth and malignant transformation. c Invasion assays were performed in A2780, SKOV3 and HO8910 cells with Rad50 overexpression or knockdown. **P<0.01, ***P<0.001. d Morphological changes of A2780 cells with Rad50 overexpression or knockdown. E, EMT-related markers

were detected by western blot in A2780, SKOV3 and HO8910 cells with Rad50 overexpression or knockdown.

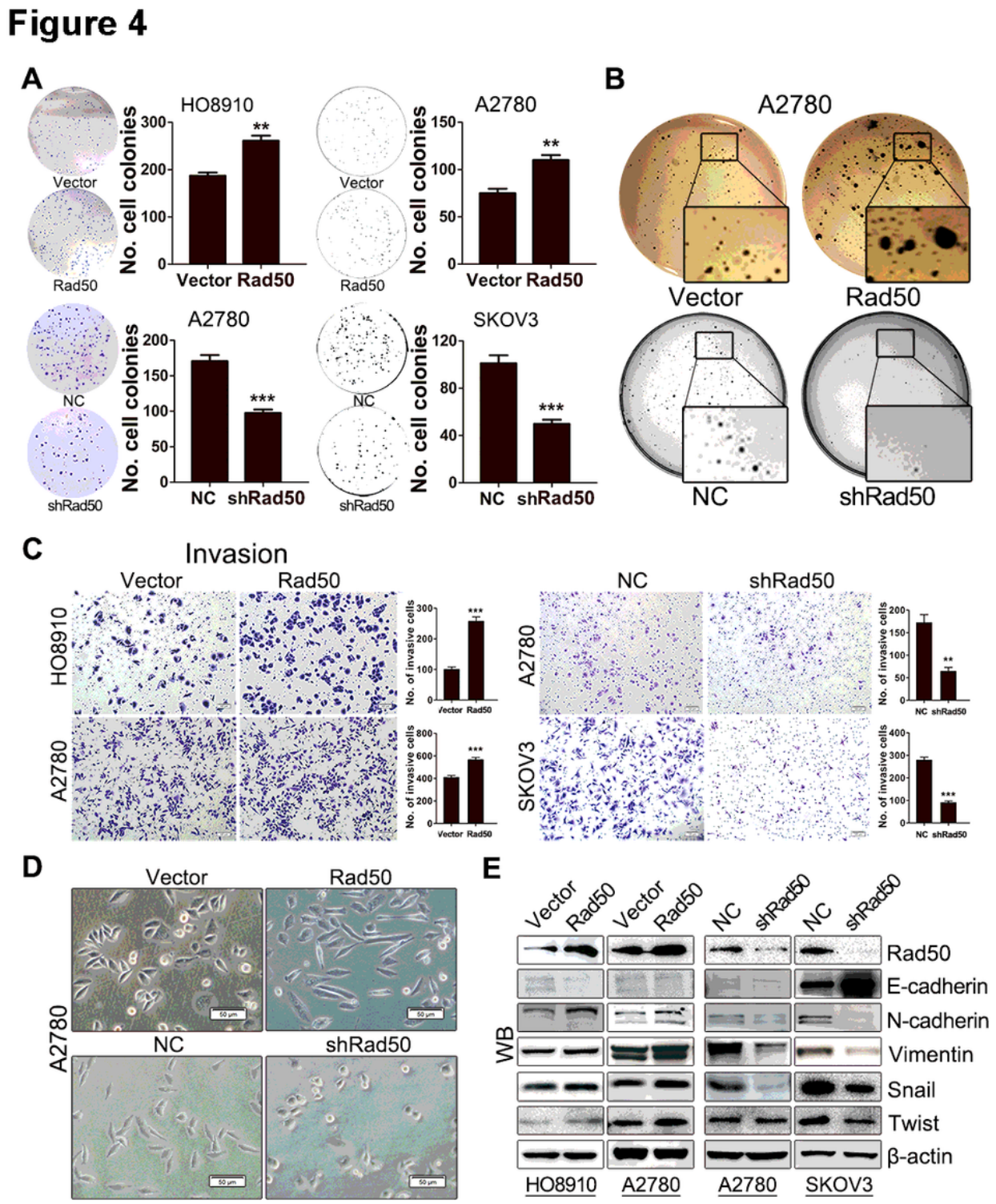

Figure 4

Rad50 promotes proliferation and invasion of ovarian cancer cells. a Effect of Rad50 on clonogenic ability in ovarian cancer cell lines. b Soft agar colony formation assay exhibited the effect of Rad50 on anchorage-independent growth and malignant transformation. c Invasion assays were performed in

A2780, SKOV3 and HO8910 cells with Rad50 overexpression or knockdown. **P<0.01, ***P<0.001. d Morphological changes of A2780 cells with Rad50 overexpression or knockdown. E, EMT-related markers were detected by western blot in A2780, SKOV3 and HO8910 cells with Rad50 overexpression or knockdown.

Figure 4

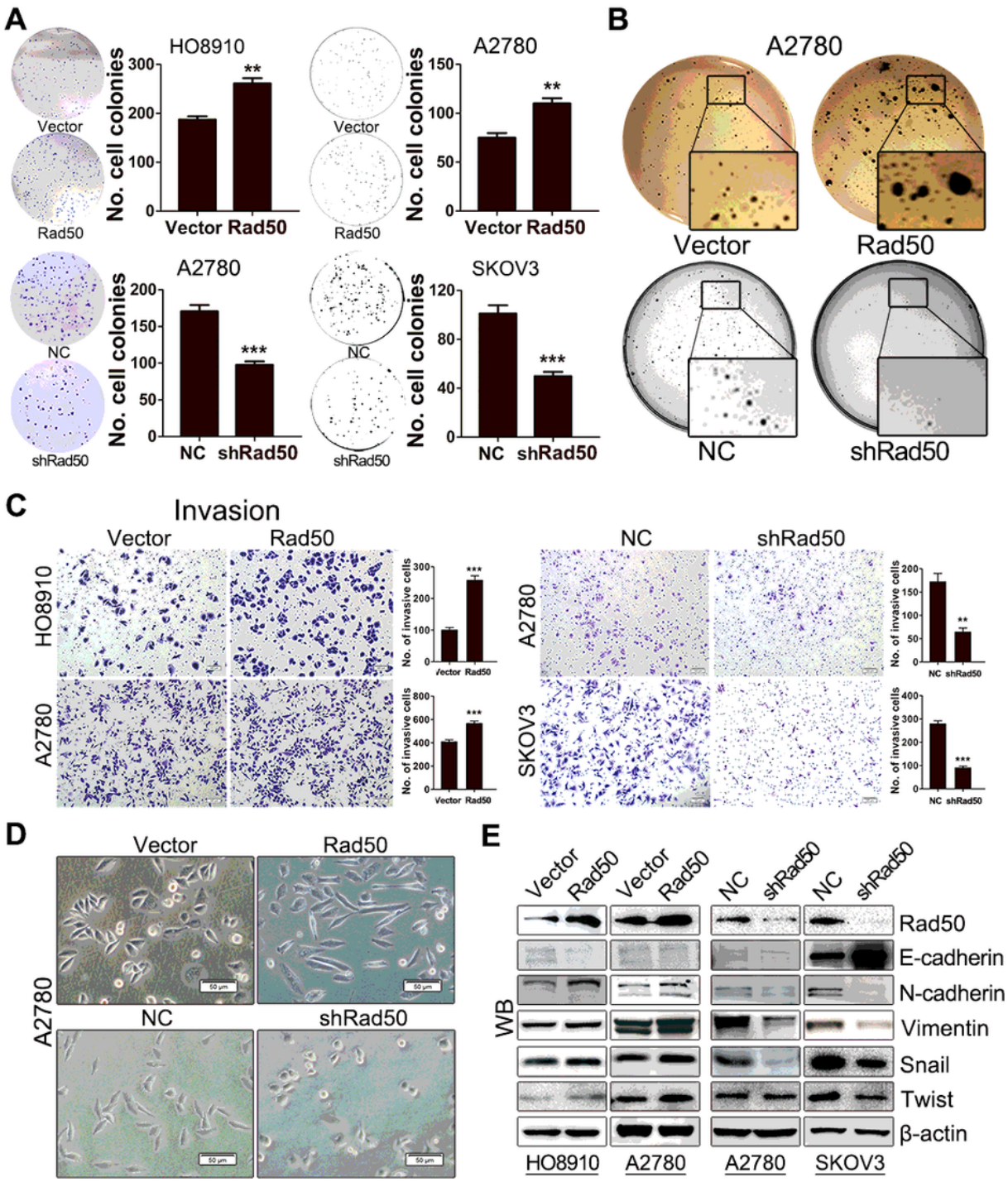

Figure 4

Rad50 promotes proliferation and invasion of ovarian cancer cells. a Effect of Rad50 on clonogenic ability in ovarian cancer cell lines. b Soft agar colony formation assay exhibited the effect of Rad50 on anchorage-independent growth and malignant transformation. c Invasion assays were performed in A2780, SKOV3 and HO8910 cells with Rad50 overexpression or knockdown. **P<0.01, ***P<0.001. d Morphological changes of A2780 cells with Rad50 overexpression or knockdown. E, EMT-related markers were detected by western blot in A2780, SKOV3 and HO8910 cells with Rad50 overexpression or knockdown.

Figure 5

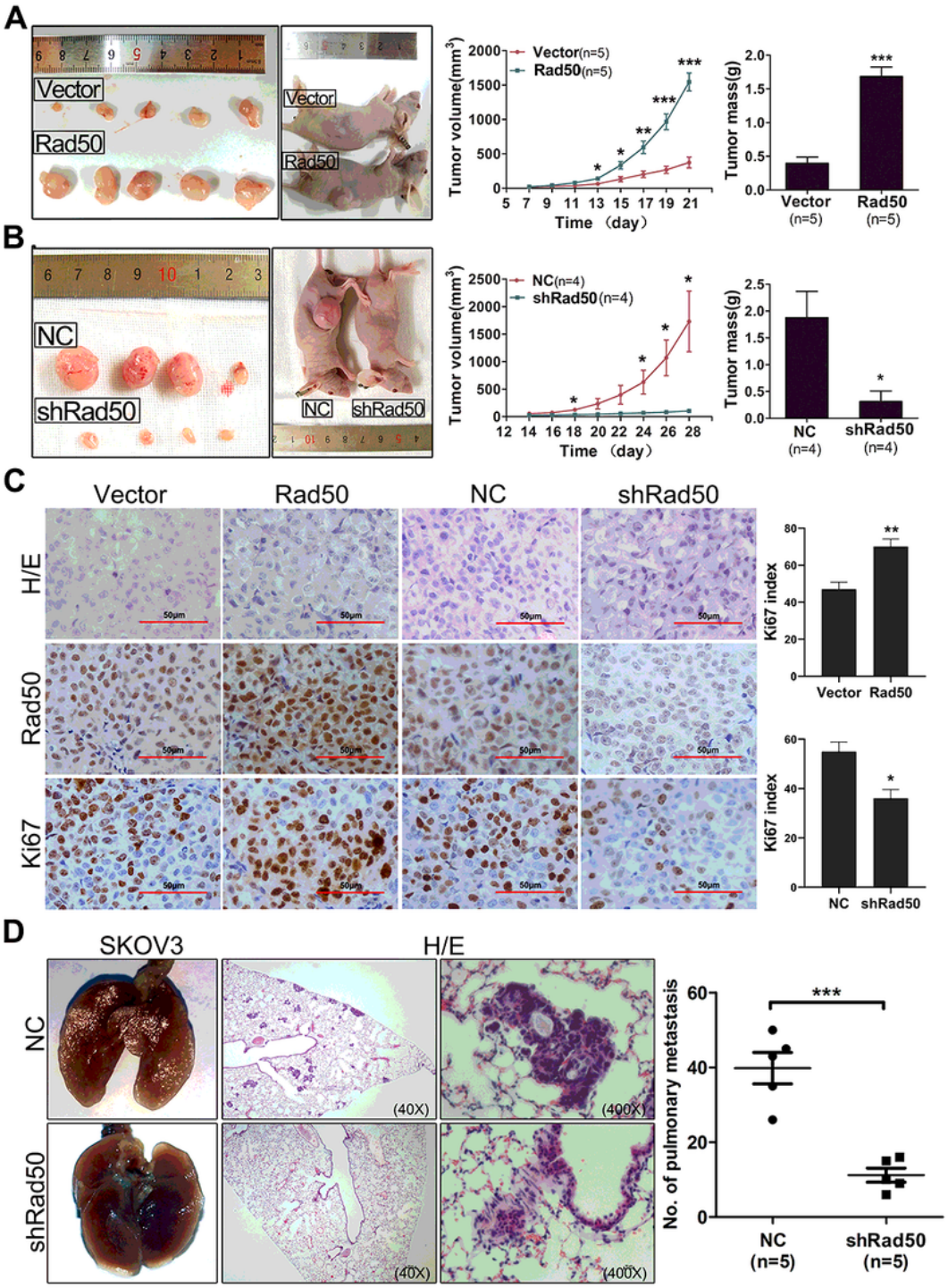

Figure 5

Rad50 promotes growth and metastasis of tumor xenografts. a-b Photographs illustrated tumors in xenografts via subcutaneous injection of A2780 cells with Rad50 overexpression or knockdown. c Representative images of HE staining and IHC staining with indicated antibodies of tumors isolated from mice. d Representative images of lungs and HE staining isolated from mice that received tail vein injection. *P < 0.05, **P<0.01, ***P<0.001, when compared with the control group.

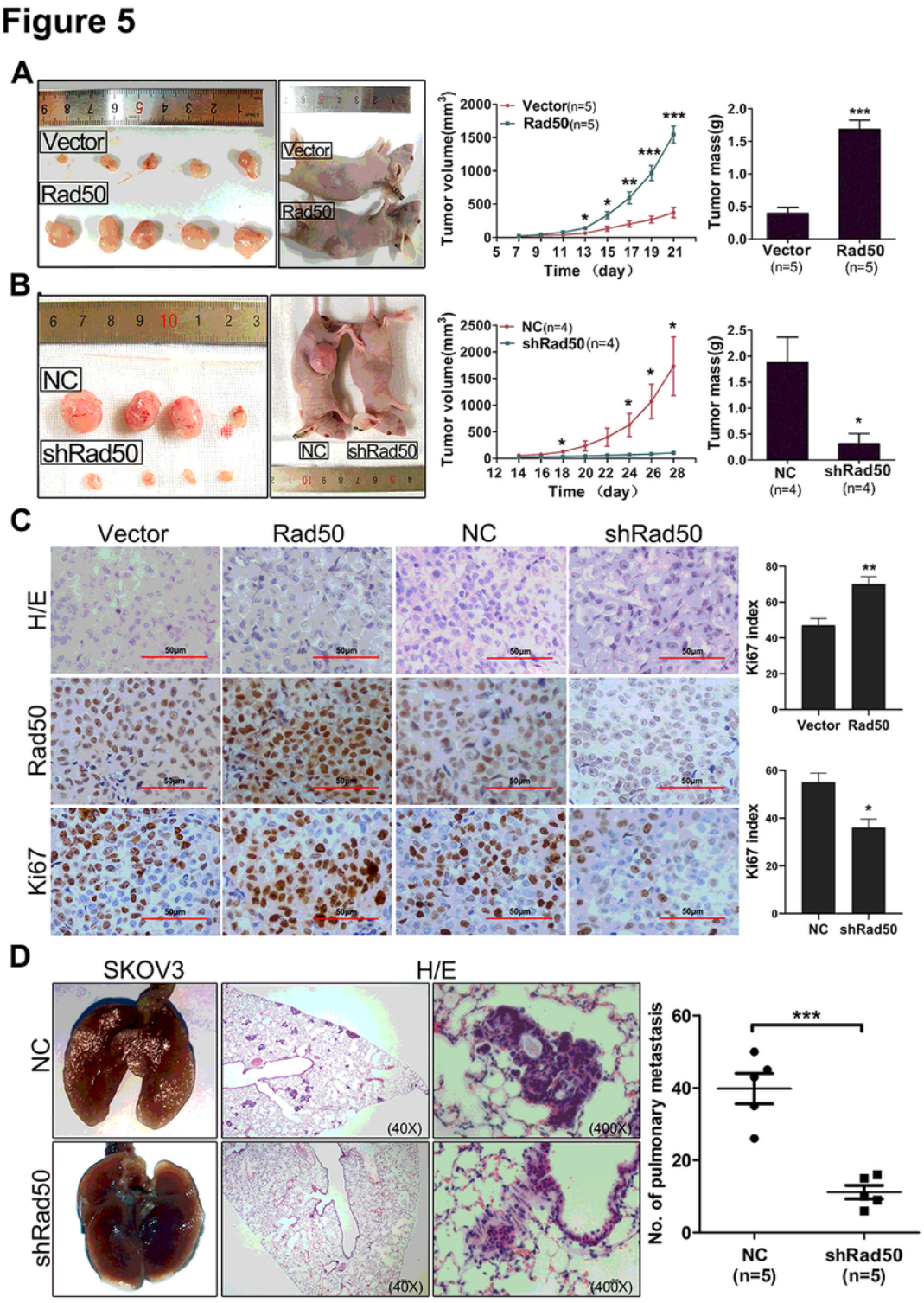

Figure 5

Rad50 promotes growth and metastasis of tumor xenografts. a-b Photographs illustrated tumors in xenografts via subcutaneous injection of A2780 cells with Rad50 overexpression or knockdown. c Representative images of HE staining and IHC staining with indicated antibodies of tumors isolated from mice. d Representative images of lungs and HE staining isolated from mice that received tail vein injection. *P < 0.05, **P<0.01, ***P<0.001, when compared with the control group.

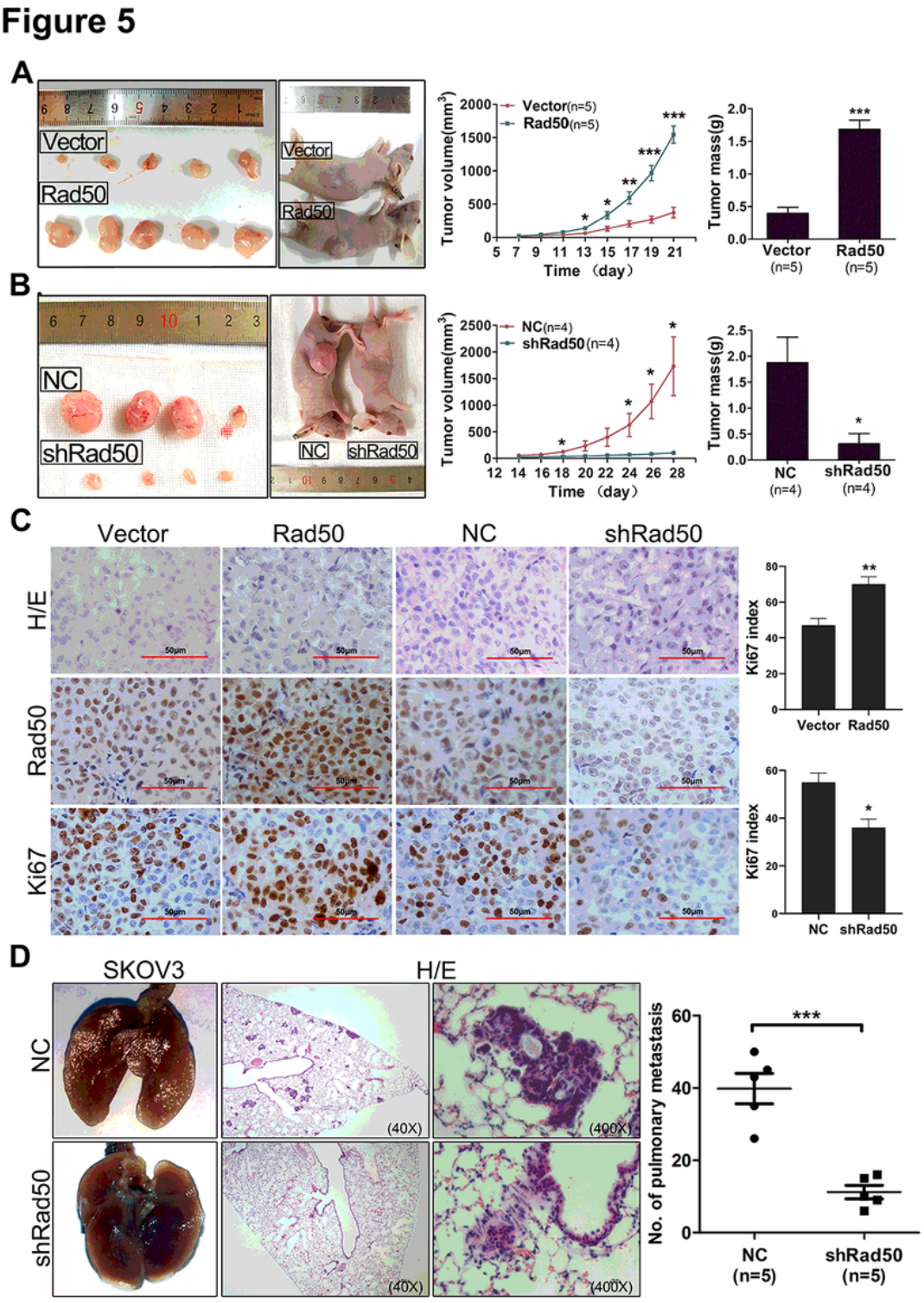

Figure 5

Rad50 promotes growth and metastasis of tumor xenografts. a-b Photographs illustrated tumors in xenografts via subcutaneous injection of A2780 cells with Rad50 overexpression or knockdown. c Representative images of HE staining and IHC staining with indicated antibodies of tumors isolated from mice. d Representative images of lungs and HE staining isolated from mice that received tail vein injection. *P < 0.05, **P<0.01, ***P<0.001, when compared with the control group.

Figure 6

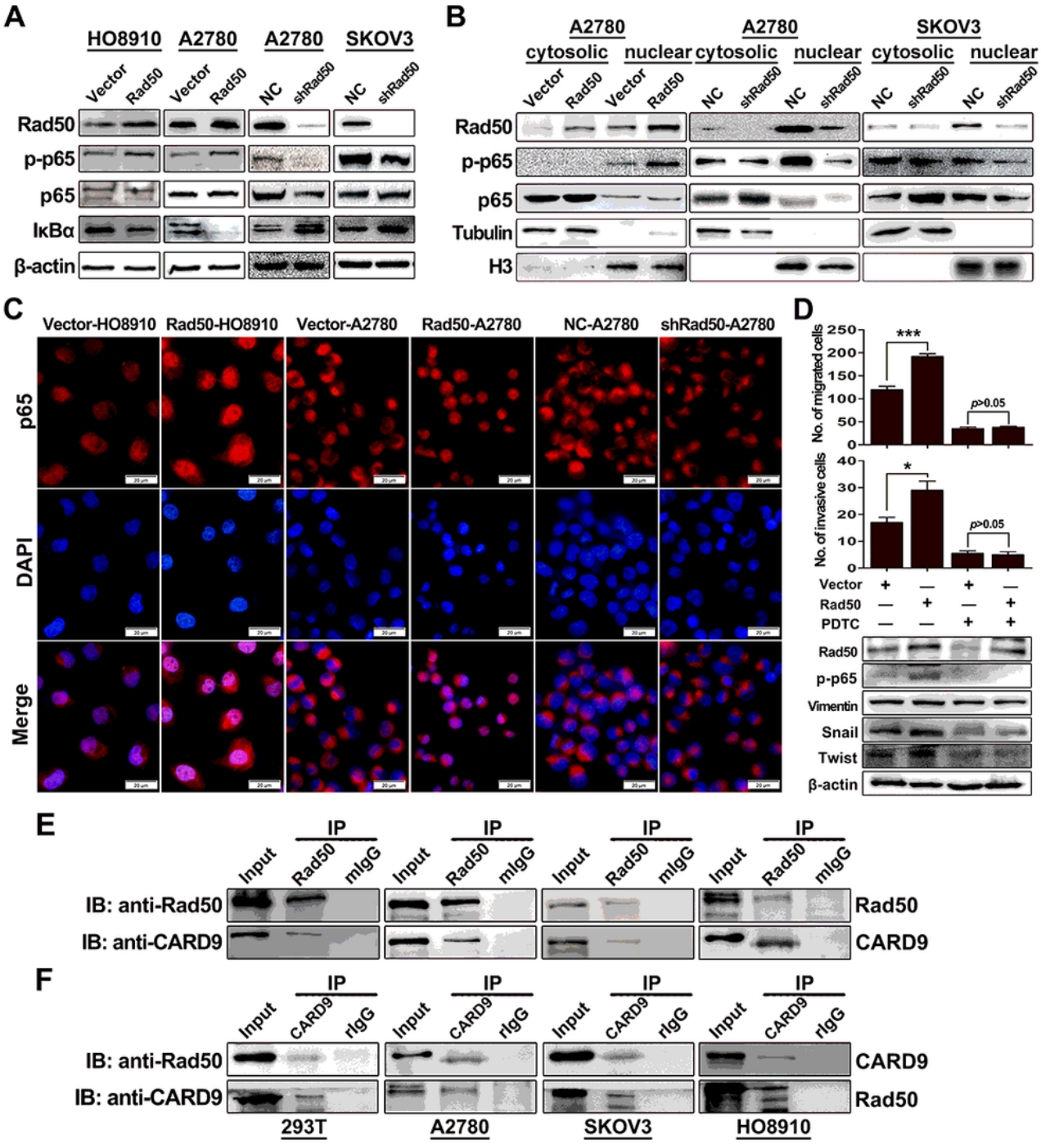

Figure 6

Rad50-mediated activation of NF-κB pathway is CARD9 dependent. a Western blot analysis showing the expression of p65, p-p65 and IκBα in ovarian cancer cell lines with Rad50 overexpression or knockdown. b Western blot analysis of indicated proteins in cytoplasmic and nuclear extracts from A2780 and SKOV3 cells with Rad50 overexpression or knockdown. c Immunofluorescence showing cytoplasmic or nuclear localization of the NF-κB complex in the indicated cell lines. d In the absence or presence of NF-κB inhibitor PDTC, migration/invasion ability and NF-κB downstream targets were measured with or without Rad50 overexpression. *P < 0.05, **P<0.01, ***P<0.001, when compared with the control group. e Interaction of Rad50 and CARD9 was determined by co-IP and western blot in HEK293T and ovarian cancer cell lines immunoprecipitated with either anti- Rad50 antibody or IgG control. f Interaction of Rad50 and CARD9 was determined by co-IP and western blotting in indicated cell lines immunoprecipitated with anti- CARD9 antibody or IgG control.

Figure 6

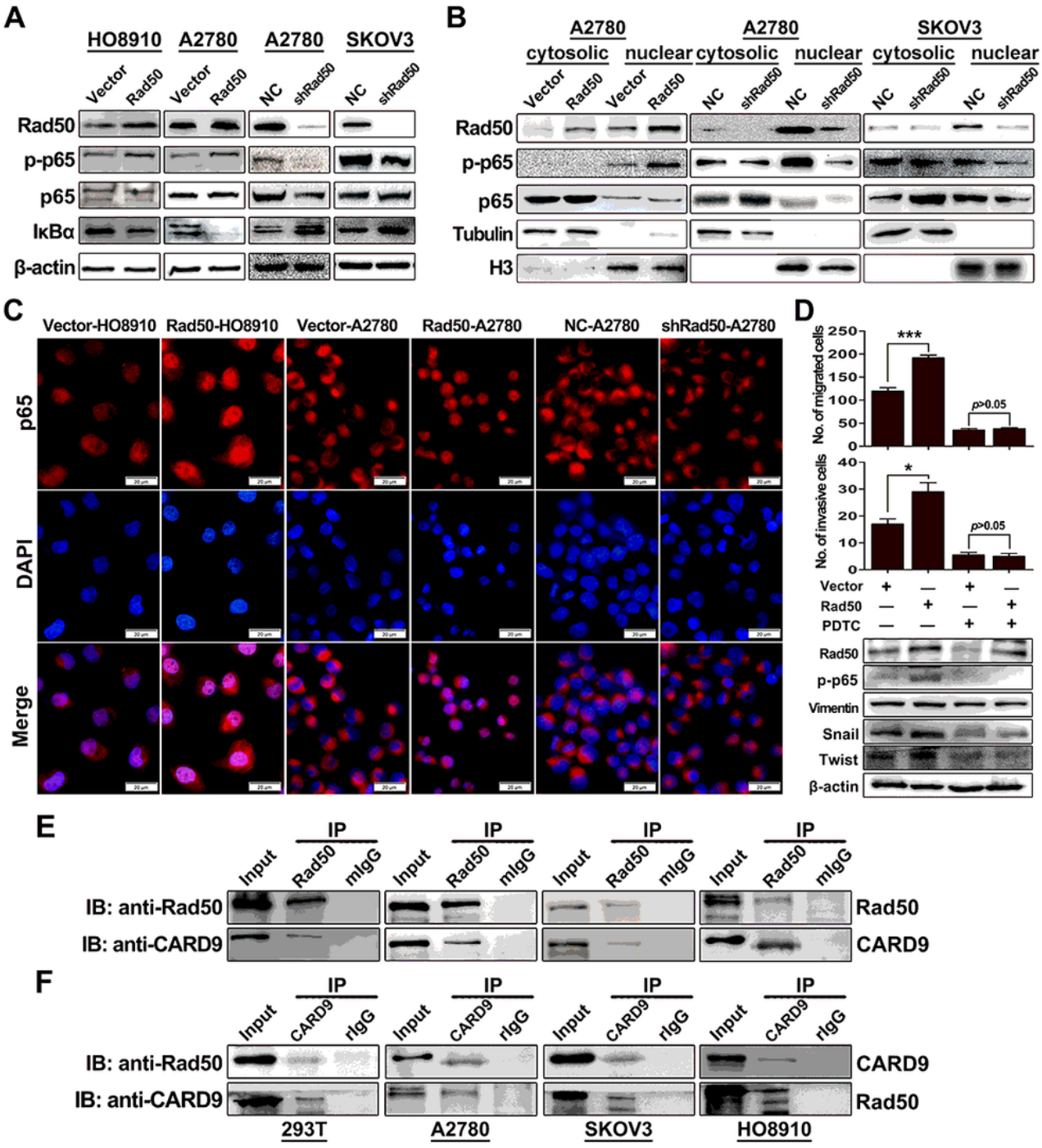

Figure 6

Rad50-mediated activation of NF-κB pathway is CARD9 dependent. a Western blot analysis showing the expression of p65, p-p65 and IκBα in ovarian cancer cell lines with Rad50 overexpression or knockdown. b Western blot analysis of indicated proteins in cytoplasmic and nuclear extracts from A2780 and SKOV3 cells with Rad50 overexpression or knockdown. c Immunofluorescence showing cytoplasmic or nuclear localization of the NF-κB complex in the indicated cell lines. d In the absence or presence of NF-κB

inhibitor PDTC, migration/invasion ability and NF-κB downstream targets were measured with or without Rad50 overexpression. *P < 0.05, **P<0.01, ***P<0.001, when compared with the control group. e Interaction of Rad50 and CARD9 was determined by co-IP and western blot in HEK293T and ovarian cancer cell lines immunoprecipitated with either anti- Rad50 antibody or IgG control. f Interaction of Rad50 and CARD9 was determined by co-IP and western blotting in indicated cell lines immunoprecipitated with anti- CARD9 antibody or IgG control.

Figure 6

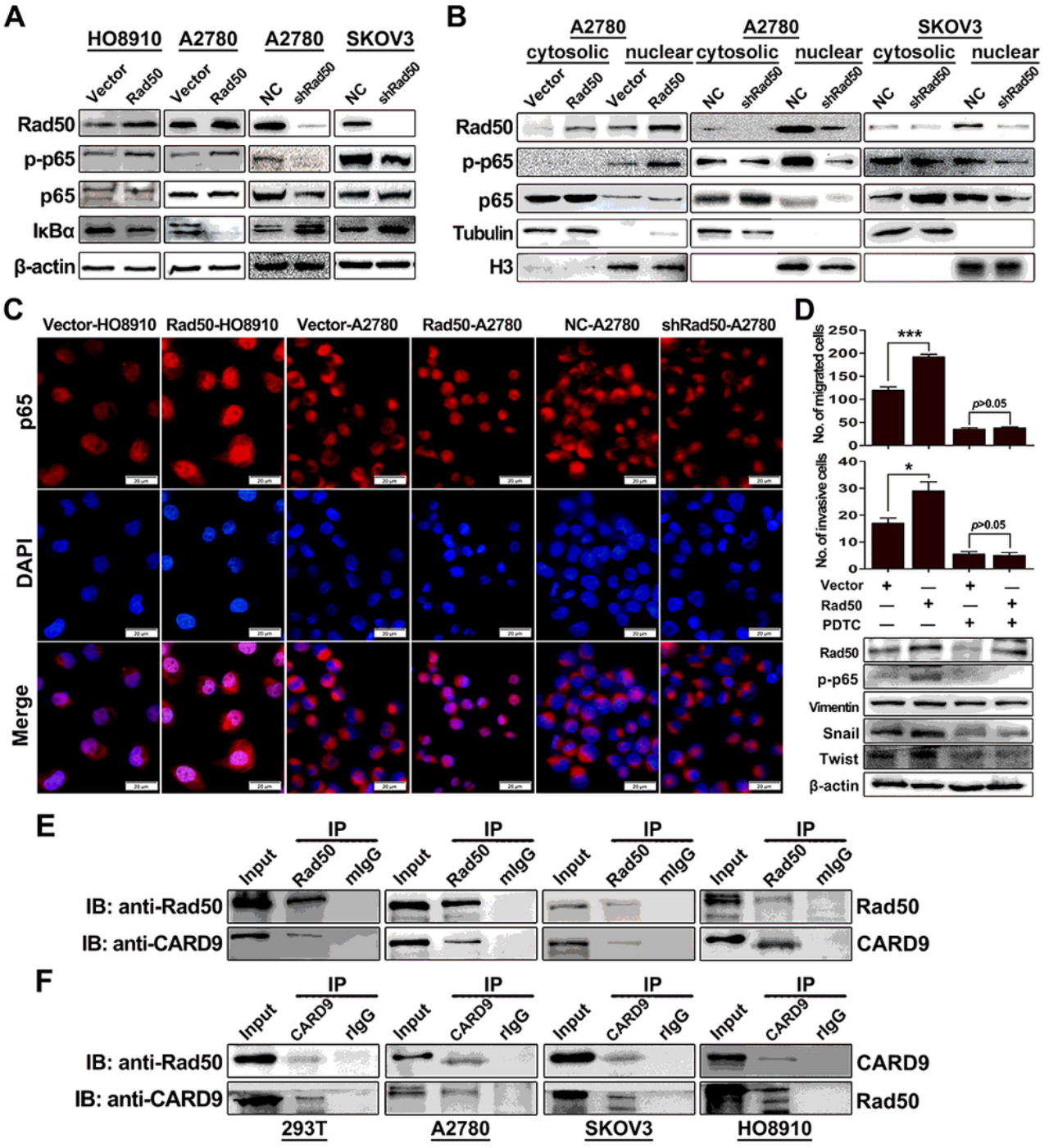

Figure 6

Rad50-mediated activation of NF-κB pathway is CARD9 dependent. a Western blot analysis showing the expression of p65, p-p65 and IκBα in ovarian cancer cell lines with Rad50 overexpression or knockdown. b Western blot analysis of indicated proteins in cytoplasmic and nuclear extracts from A2780 and SKOV3 cells with Rad50 overexpression or knockdown. c Immunofluorescence showing cytoplasmic or nuclear localization of the NF-κB complex in the indicated cell lines. d In the absence or presence of NF-κB inhibitor PDTC, migration/invasion ability and NF-κB downstream targets were measured with or without Rad50 overexpression. *P < 0.05, **P<0.01, ***P<0.001, when compared with the control group. e Interaction of Rad50 and CARD9 was determined by co-IP and western blot in HEK293T and ovarian cancer cell lines immunoprecipitated with either anti- Rad50 antibody or IgG control. f Interaction of Rad50 and CARD9 was determined by co-IP and western blotting in indicated cell lines immunoprecipitated with anti- CARD9 antibody or IgG control.

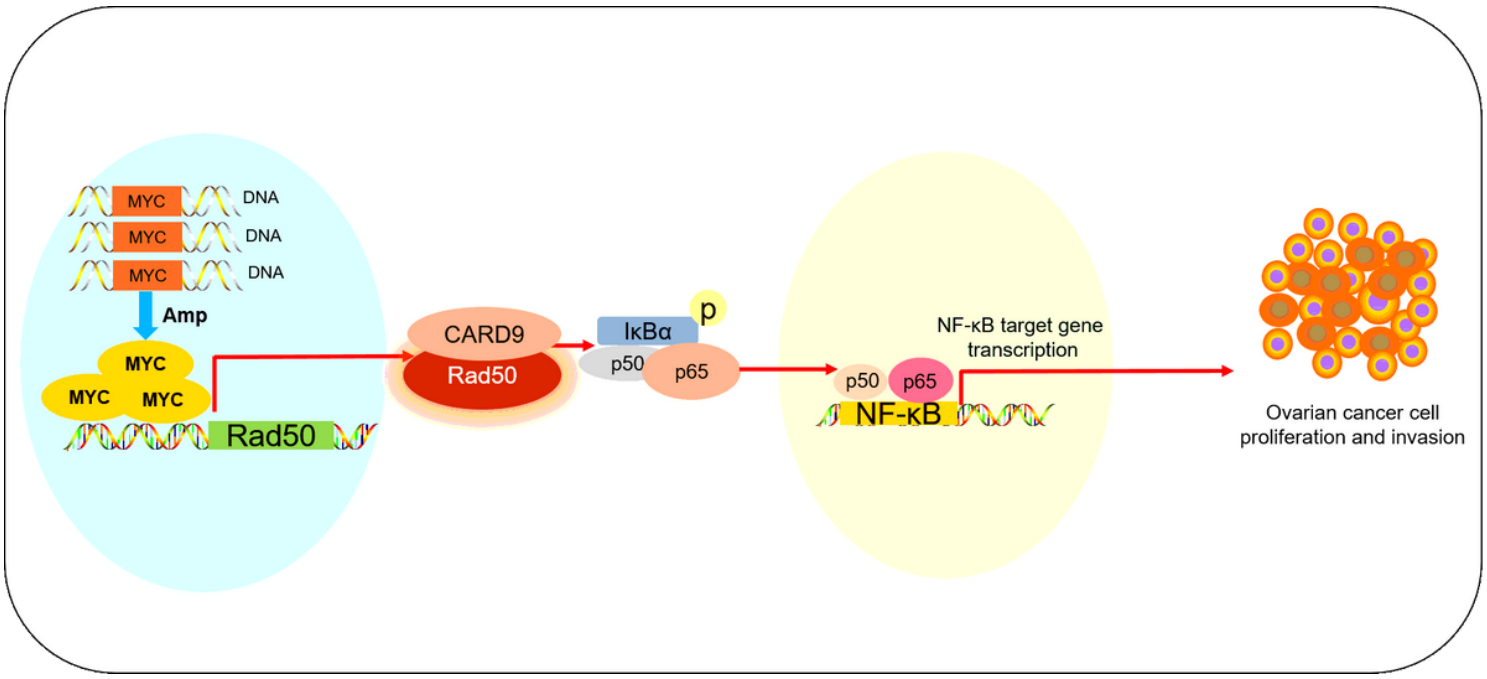

Figure 7

The diagram of the mechanism that MYC targeted Rad50 drives ovarian cancer progression via NF-κB activation.

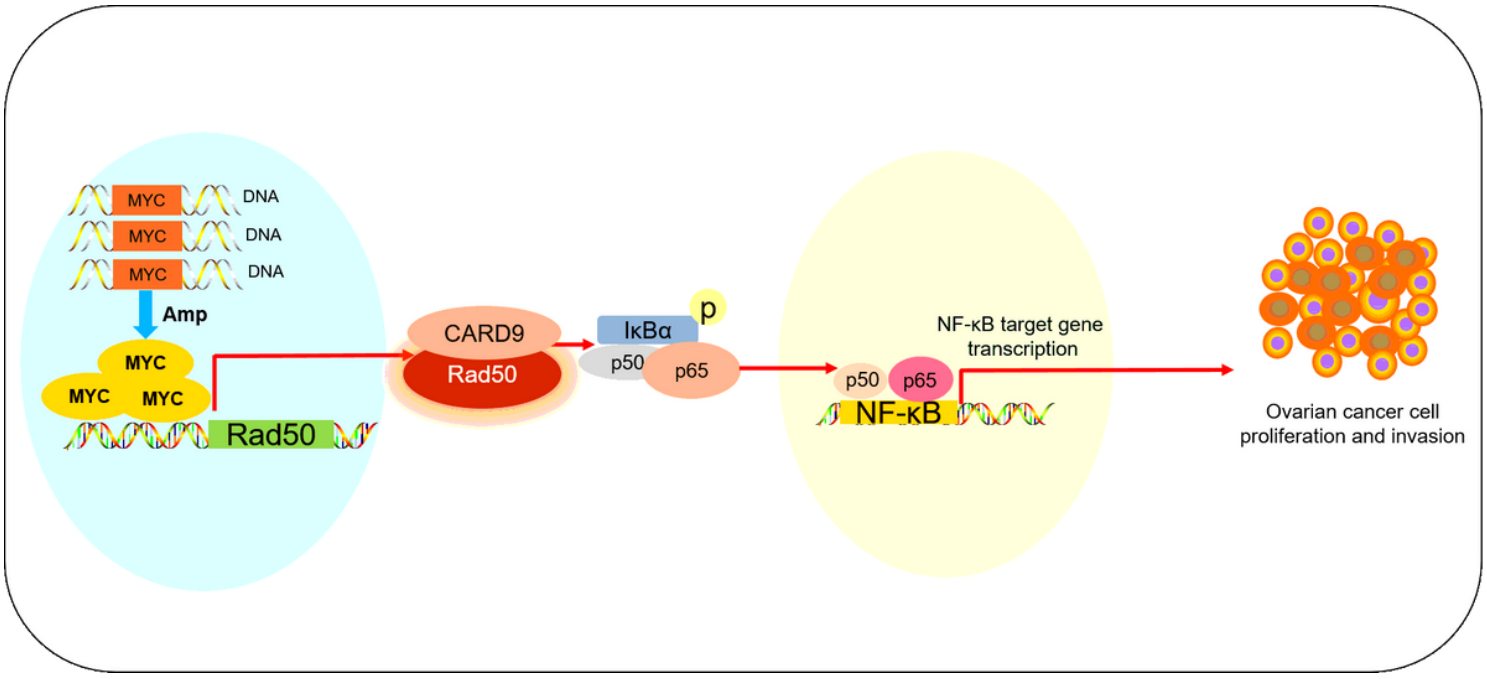

Figure 7

The diagram of the mechanism that MYC targeted Rad50 drives ovarian cancer progression via NF-κB activation.

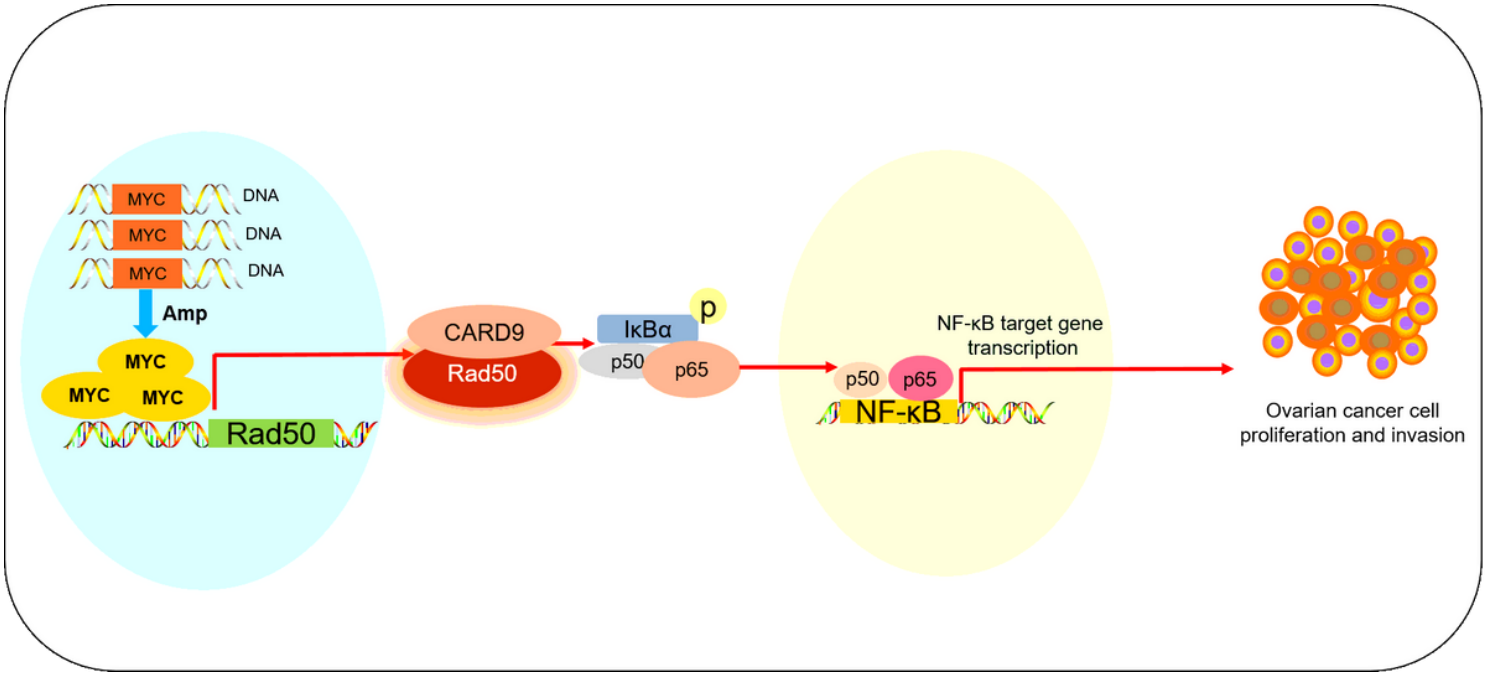

Figure 7

The diagram of the mechanism that MYC targeted Rad50 drives ovarian cancer progression via NF-κB activation.

Supplementary Files

This is a list of supplementary files associated with this preprint. Click to download.

- SupplementaryFigurelegends.docx
- SupplementaryFigurelegends.docx
- SupplementaryFigurelegends.docx
- SupplementaryFigures.docx
- SupplementaryFigures.docx
- SupplementaryFigures.docx
- SupplementaryTables.docx
- SupplementaryTables.docx
- SupplementaryTables.docx